7

Geochemistry and Metallogenic Model of Carlin-Type Gold Deposits in Southwest Guizhou Province, China

Yong Xia, Wenchao Su, Xingchun Zhang and Janzhong Liu
State Key Laboratory of Ore Deposit Geochemistry, Institute of Geochemistry
Chinese Academy of Sciences, Guiyang
China

1. Introduction

Carlin-type gold deposits, also known as sediment-hosted gold deposits are among the largest hydrothermal gold deposits in the world, currently being sought and mined in the United States and China (Tretbar et al., 2000; Hu et al., 2002). The region of southwestern Guizhou (SW Guizhou), which is a region where the Carlin-type gold deposits were found for the earliest time in China, is an important component of the Yunnan-Guizhou-Guangxi "gold triangle" province. Carlin-type gold deposits in SW Guizhou, China, are hosted in late Paleozoic and early Mesozoic sedimentary rocks along the southwest margin of the Precambrian Yangtze craton. They can be classified as two types, i.e., the fault type and the strata-bound type, on the basis of their occurrence, shape and structural controls (Zhang et al., 2003; Xia, 2005). The former type includes the Lannigou, Yata, Banqi, Zhimudang (the upper orebodies), etc. with gold ores mostly occurring in high-angle compresso-shear faults. The ore-hosted strata are generally Middle and Lower Triassic in age, ore-bearing rocks are dominated by muddy siltstones and silty mudstones. The strata-bound gold deposits include the Shuiyindong, Taipingdong, Zhimudang (the lower orebodies), Getang, Nibao, etc. Gold ores are hosted mainly in the interbeded rupture zone at the karst discontinity surface of the Upper-Lower Permian and the Upper Permian strata. The deposits are mostly concealed ones at depth, the orebodies occur as stratiform, stratoid and lenticular ones and are developed along the strata, characterized by multi-layer distribution. Ore-hosted rocks are mainly impure bioclastic limestones and carbonate rocks in organic-rich coal series formations, with obvious anticline ore-controlling features. They have characteristics similar to Carlin-type gold deposits in Nevada, including notable enrichment in As, Sb, Hg, and Tl (Hu et al., 2002; Xia, 2005). Typical characteristics include impure carbonate or calcareous and carbonaceous host rock that contains disseminated pyrite and arsenopyrite. Gold occurs either as submicrometer-sized particles or invisibly as solid solution in As-rich rims of pyrite and arsenopyrite. Late stibnite, realgar, and orpiment fill fractures on the periphery of gold mineralization. Hydrothermal alteration caused decarbonation, silicification, argillization, and sulfidation, similar to Carlin-type gold deposits in Nevada (Hofstra and Cline, 2000; Emsbo et al., 2003; Kesler et al., 2003). Detailed studies in recent years have shed much light on the geochemistry and metallogenic mechanisms of the Carlin-type gold deposits in the

region, promoted metallogenic prognosis and exploration, thus making the Shuiyindong gold deposit become a typical super-large Carlin-type gold deposit. On the other hand, a great breakthrough has been made in metallogenic prognosis and exploration of Carlin-type gold deposits on a regional scale.

2. Regional geologic setting

2.1 Stratigraphy in SW Guizhou

The Carlin-type gold mineralization area in southwestern SW Guizhou Province (Fig.1) lies on the southwestern edge of the Yangtze Paraplatform which is composed of crystalline rocks of Proterozoic age overlain mainly by shallow-marine platform deposits of Devonian through Triassic age. After the Caledonian tectonism, from Devonian to Triassic, this area subsided and formed a large sedimentary basin filled with thick sedimentary strata. Outcrops of Devonian, Carboniferous, Permian and Triassic strata occur in the area with sporadic outcrops of Jurassic and Cretaceous strata in this area.

The Carlin-type gold in SW Guizhou are located in sedimentary rocks of Permian and Triassic age, and the environment of sedimentation changed from continental, to marine platform to marine basin facies across the area from the northwest, to the central and to the southeastern part.

The Permian strata are mainly limestones of the Lower Permian with EW-trending facies distribution, and clastic sediments and thinly-bedded limestones of the Upper Permian with NS-trending facies distribution. Late Permian strata change from the northwest to the southeast across the line of Anshun-Anlong-Xingyi. On the northwest side of the line, there are interbedded continental margin facies, where the Getang deposit is located on the palaeokarst surface which separates Early and Late Permian sequences. On the southeast side, there are mainly platform carbonates, and reef facies along the platform margin. Further to the southeast, sedimentation took place in a deep-sea trough-like basin near Ceheng-Zhenfeng-Ziyun-Wangmo and shingle fine-grained clastic sediments of the marine basin were deposited.

Triassic strata were developed extensively in the area. The Late Permian framework of sedimentation continued into the Early Triassic period. The Early Triassic platform facies, mainly marl and claystone interbedded with bioclastic limestone, in which the Zimudang deposit is located, is situated on the northwest side of the Anshun-Zhenfeng-Ceheng line. However, a slope facies of platform margin, mainly calcirudite and micritic limestone, occurs on the southeast side, and the marine basin facies, micritic limestone and shale, occurs further to the southeast. The Banqi and Ceyang deposits are located in slope facies which surrounded the Permian island reef.

The pattern of sedimentation of the Early Triassic continued through the Middle Triassic. The Middle Triassic slump deposits of conglomerate/psephite which crop out in the belt between the platform margin and the deep-sea trough-like basin further indicate that it was an active fault-trough basin. The Lannigou and Yata deposits are located on the boundary between that belt and deep-sea facies. There were Middle Triassic platform facies on the northwest side of the platform margin along the line of Anshun-Zhenfeng-Ceheng, and marine basin facies on the southeast side.

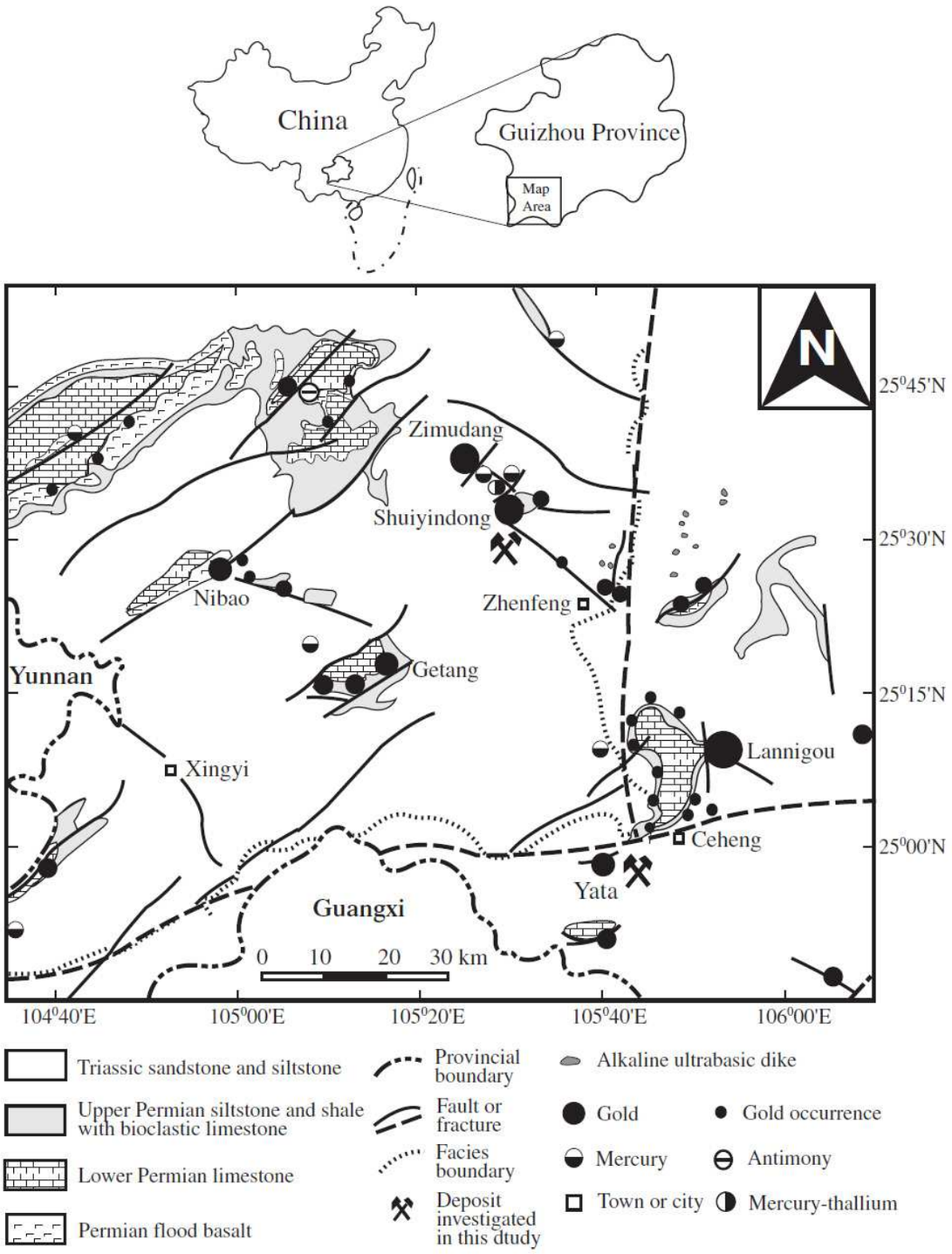

Fig. 1. Simplified geologic map of southwestern Guizhou (modified after Zhang et al., 2003), showing the locations of the major Carlin-type gold (e.g., Shuiyindong and Yata) and antimony and mercury deposits.

2.2 Igneous rocks in SW Guizhou

Outcrops of both intrusive and extrusive igneous rocks including basalts, diabase, vitric tuff and meta-alkaline ultrabasic rocks occur in the area (Fig.2). Several sequences of basalts from Carboniferous to Late Permian are exposed in in the northwest corner of the area. Explosion-type basalts of Early Carboniferous and Early Permian only crop out locally in shallow marine environment, whereas Late Permian Emeishan basalts of the continental flood-type are widely exposed on the northwest corner of the area with the thickness of the basalt sequence decreasing from west (500-1250m in Panxian/Puan) to east (<150m in Anshun/Qinglong) (Bureau of Geology and Mineral Resources of Guizhou Province, 1987; Yang et al., 1992; Li et al., 1989). From the results of petroleum exploration drilling, it is known that a thick sequence of Late Permian Emeishan basalts, reaching one thousand metres, lies buried several hundred metres beneath the western area of Xingyi and Luoping (Huang, 1986). Late Permian diabases are generally exposed as sills and dykes in limited areas (Mei, 1973, 1980). Thin seams of Late Permian acidic vitric tuffs are locally distributed within Triassic dolomite and claystone. Small pipes and dykes of meta-alkaline ultrabasic rocks are exposed in the belt of transitional sedimentary facies along the line of Zhenfeng-Ziyun (Mei, 1973). It is believed that the Puding-Ceyang Fracture provided a pathway for their intrusion (Yang et al., 1992).

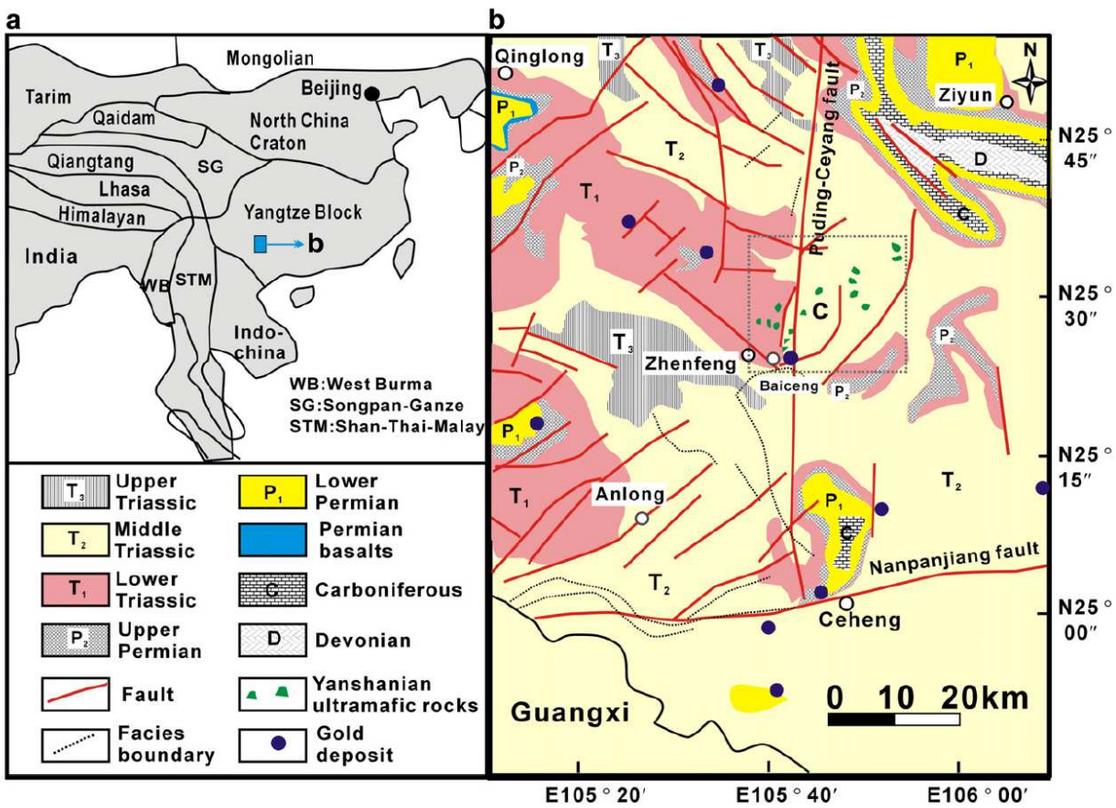

Fig. 2. (a) Distributions of the major terranes in China (modified after Chung and Jahn, 1995); (b) geological map of the SW Guizhou area and the distribution of the sedimentary rocks, Permian basalts, tectonic elements, ultramafic dykes and gold deposits.

2.3 Regional structures in SW Guizhou

The SW Guizhou lies on the southwestern edge of the Yangtze Paraplatform. The adjacent southeast area (mainly northwestern Guangxi) belongs to Youjiang geosyncline which is believed to be the northwest part of the South China Fold System. However, with the discovery of characteristic Yangtze paraplatform-type sedimentary associations, fossils and Caledonian folds in covering strata, it is believed that the Youjiang geosyncline was developed on the southwestern edge of the Yangtze Paraplatform by continental rifting activation during the Variscan cycle (Lu, 1986).

Several deep fractures or fracture zones cut through the area (Fig.1, Fig.2). The movements on these fractures provided an important control on geological development including sedimentation and folding in this area from Late Palaeozoic to Triassic time (Li et al., 1989, Yang et al., 1992, Hou and Yang, 1989). The NE-trending Mile-Shizhong Fracture cut through the nortwestern part of the area and separates the outcrop of Upper Proterozoic sediments and Permian continental flood basalts on its northwest side from the Triassic sediments on its southeast side. The NW-SE-trending Shuicheng-Ziyun-Bama Fracture Zone (Hezhang-Ziyun) cut through the northeast part of the area. The NEE-trending Nanpanjiang Fracture (Kaiyuan-Pingtang) cut through the southern part of the area with the character of different Triassic sedimentary facies on its two sides. The NS-trending Puding-Ceyang Fracture is believed to be a concealed fracture with the characteristic outcrop of meta-alkaline ultrabasic pipes and the characteristic sedimentary transition of Permian and Triassic strata along the line (Yang et al., 1992). However, Wang et al. (1994) indicated that the boundary between clastic rocks and carbonates along the line of Anshun-Zhenfeng-Ceyang-Nidang was not a real sedimentary transition boundary but a SW Guizhou Thrust formed by thrusting of the shallow-water carbonates onto the calstic sediments from nothwest to southeast after the main gold mineralization, with possible maximum thrusting distance of 80 km at peak of the thrust arc near Ceyang.

As a result of the reactivation of these fractures during the Yanshanian orogeny from Middle Triassic to the end of the Cretaceous, a series of subsidiary fractures were formed. It was with these that the gold, mercury, antimony and arsenic mineralization were associated. According to the characteristic sedimentary associations, the structural deformation of the sedimentary cover and the distribution of regional deep fracture zones in this area, two structural units are identified by the Bureau of Geology and Mineral Resources of Guizhou Province (1987). The Puan Rotational-Shear Deformation Area, which is bordered by the Nanpanjiang Fracture to the south, the Puding-Ceyang Fracture to the east and the Shuicheng-Ziyun Fracture to the northeast, mainly has rotational-shear folds associated NW-, NE- and NNE-trending structures, carbonates and calcareous clastic sediments with coal seams of carbonate platform facies in which the gold deposits of Getang, Zimudang, Sanchahe, Xiongwu, the Lamuchang mercury-thallium deposit and the Dachang antimony deposit are located. The Wangmo Deformation Area, which is bordered by the Ziyun-Bama Fracture to the northeast and the Puding-Ceyang Fracture on the west, mainly has NW-trending shear structures and EW- and NS-trending compressive structures, turbidites of marginal slope facies and marine basin facies in which the gold deposits of Banqi, Yata, Baidi, Lannigou, Daguan are located.

3. Geology of the gold deposits

There are two kinds of Carlin-type gold deposits: stratabound and fault-controlled in the southwestern Guizhou Province. The stratabound Carlin-type gold deposits such as Shuiyindong, Taipingdong, Zimudang (lower orebodies), Getang, Nibao gold deposits, etc. are controlled by anticlines and hosted in silty bioclastic limstones of Upper Permian (e.g., Shuiyindong). The fault-controlled Carlin-type gold deposits such as Lannigou, Yata, Banqi, Zimudang (upper orebodies) gold deposits, etc. are localized at the compressive shear faults and hosted in siltstones and silty mudstones of Middle or Lower Triassic (e.g., Yata).

3.1 Geology of the Shuiyindong (Stratabound Carlin-type gold deposit)

The Shuiyindong deposit is located about 20 km northwest of the town of Zhenfeng in southwestern Guizhou (Fig. 3). It lies on the eastern limb of the Huijiabao anticline (Fig. 3A), which also hosts a cluster of deposits on its western limb, including the Zimudang deposit. Recent exploration and mining at Shuiyindong has proven gold reserves of 55 metric tons (t) Au (1.8 Moz), with average gold grades from 7 to 18 g/t (Xia, 2005). All of the gold is refractory, occurring in arsenian pyrite and arsenopyrite (Xia, 2005; Su et al., 2008).

Sedimentary rocks in the district consist of bioclastic limestone, siltstone, and argillite of the Middle and Upper Permian and Lower Triassic. The Middle Permian Maokou Formation, a massive bioclastic limestone, is overlain by the Upper Permian Longtan, Changxing, and Dalong and Lower Triassic Yelang Formations. The Longtan Formation is about 300 m thick in the Shuiyindong district and has been divided into three stratigraphic units (Liu, 2001). The lowest unit consists of calcareous siltstone, which grades into fine-grained sandstone at the top. The second unit consists of silty argillite intercalated with bioclastic limestone and coal seams. The third unit includes calcareous siltstone, sandstone, and muddy and bioclastic limestone. Gold mineralization is preferentially disseminated in bioclastic limestone and calcareous siltstone of the first and second units of the Longtan Formation at depths of 100 to 300 m below the surface (Fig. 3B). These rocks were deformed into an east-trending anticline with limbs that dip 10° to 20°. Strata-bound gold orebodies are located mainly on the flanks of the anticline (Fig. 3B). The limbs of the anticline are cut by reverse faults F101 and F105, respectively, which strike east-west and dip steeply to the north and south, respectively (Fig. 3A). The reverse faults host small orpiment and realgar bodies with low-grade gold mineralization and are cut by a series of near northsouth–trending normal faults with steep dips (70°–80°). The normal faults contain mercury-thallium deposits, such as Lanmuchang (Fig. 3A).

The three main orebodies at Shuiyindong (IIIa, IIIb, IIIc; Fig. 3B) contain approximately half of the gold reserves. They are 100 to 400 m long, 50 to 350 m wide, 1.7 to 1.9 m thick, and have an average gold grade of 16 g/t (Xia, 2005). A lower grade orebody (Ia) is hosted in silicified, brecciated argillite and limestone at the unconformity between the Maokou Limestone and the first unit of the Longtan Formation. This unconformity controlled the distribution of other gold deposits regionally in the southwestern Guizhou, such as Getang and Nibao (Fig. 1), suggesting that it may have been a feeder conduit for gold mineralization.

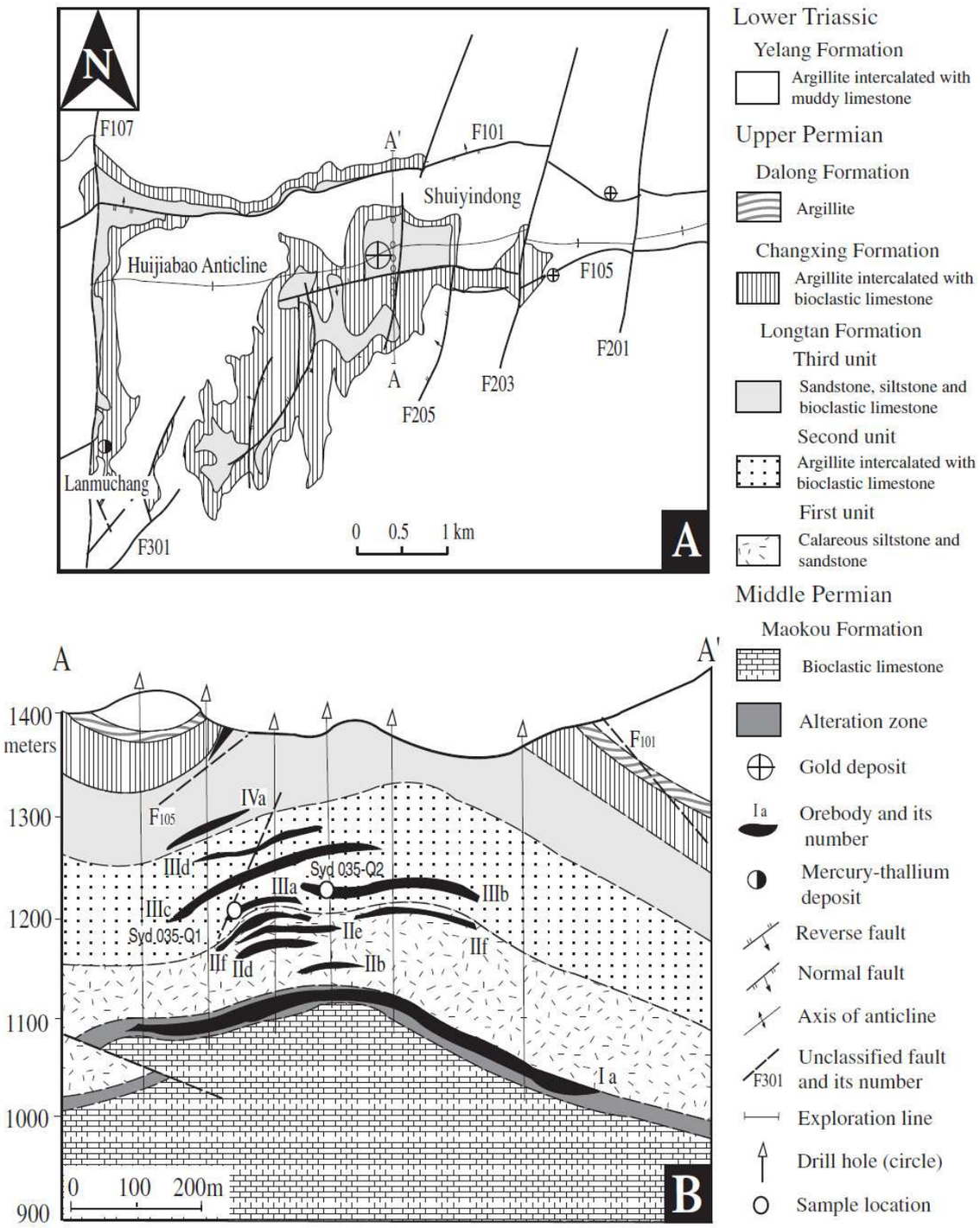

Note the stratiform nature of the numbered orebodies.

Fig. 3. Simplified geologic plan (A) and cross section (B) along the A-A' exploration line of Shuiyindong (modified from Liu, 2001).

Wall-rock alteration at Shuiyindong caused decarbonation, silicification, sulfidation, and dolomitization. Of the alterations, silicification, dolomitization, pyritization (associated with arsenopyritization) are most closely connected with gold mineralization. In the ores metallic minerals include pyrite, arsenopyrite, hematite, stibnite (occasionally seen), cinnabar (occasionally seen), realgar (occasionally seen), and native gold (occasionally seen, found for the first time in this study) (Su Wenchao et al., 2006). Gangue minerals are quartz, dolomite, calcite, hydromica, sericite, kaolinite, and organic carbon. As viewed from the compositional characteristics of ore minerals and phase analyses, it is known that pyrite and arsenopyrite are the carrier minerals of gold.

3.2 Geology of the Yata (Fault-controlled Carlin-type gold deposit)

The Yata gold deposit is located about 15 km southwest of the town of Ceheng in southwestern Guizhou (Fig. 1). The deposit had been mined for arsenic (realgar) at a small scale for many years. Gold mineralization was discovered as a result of reconnaissance sampling around the old realgar pits in the early 1980s. Intensive exploration was carried out by the Guizhou Bureau of Geology and Mineral Resources in the late 1980s. This resulted in the definition of more than 10 t of gold reserves, with an average gold grade of 3 to 5 g/t (Tao et al., 1987). Geologic descriptions of the deposit were given by Zhang et al. (2003).

Sedimentary rocks exposed in the district are mainly siltstone, sandstone, argillaceous limestone, and shale of the Middle Triassic Xuman Formation, which is divided into four members based on sand grain size and bedding thickness (Tao et al., 1987). Gold mineralization occurs in Member 2, which is composed of interbedded sandstone, fine-grained sandstone, siltstone, and mudstone. Unmineralized carbonaceous shale in this formation contains quartz, biotite, ferroan dolomite, illite, calcite, and minor fine-grained diagenetic pyrite.

Gold mineralization (Fig.4) occurred along a narrow easttrending zone and comprises more than 40 orebodies. Most of them occur along high-angle and strike-slip faults that cut the south limb of the east-trending Huangchang anticline and subsidiary folds. Limbs of the anticline dip at 35° to 70°, contain chevron folds and mesoscopic compressive fracture zones. Faults F1, F2, F3, and F6 controlled mineralization within the zone. The F2 and F3 faults, which have easterly trends and dip south at 65° to 85°, controlled the largest mineralization zone (M1) in the district. The M1 zone is 1,500 m long, 40 to 60 m wide, and 200 m thick, with average gold grades varying from 1 to 3 g/t (Zhang et al., 2003). Smaller orebodies with average gold grades of 3 to 5 g/t occur as lenticular zones, veins, and vein stockworks within the larger envelope of mineralization. Gold orebodies are preferentially hosted in altered calcareous siltstone and shale at intersections with high-angle faults that focused fluid flow during gold mineralization.

Despite the stronger structural control than at Shuiyindong, wall-rock alteration at Yata is similar and extends well away from faults and fractures along more reactive or permeable clastic strata or calcareous shale and siltstone. Carbonate dissolution mostly occurred in carbonate strata. In proximal zones of carbonate dissolution, disseminated irregular or euhedral crystals of orpiment or realgar formed locally in porous decarbonated rocks. Silicification typically produced small bodies of jasperoidal quartz within the larger areas of altered rocks. Coarser quartz crystals occur in veins and veinlets. Argillization has mainly

produced illite or illite-quartz veinlets, many of which contain pyrite and arsenopyrite. The dominant primary ore minerals at Yata are arsenian pyrite, arsenopyrite, marcasite, stibnite, orpiment, and realgar (Zhang et al., 2003). Trace amounts of sphalerite, galena, and chalcopyrite also occur. Gangue minerals include quartz, dolomite, calcite, and clay minerals (e.g., illite). Pyrite is the dominant sulfide in the ores (3–5 vol %). It occurs disseminated in the host rocks as rounded pentagonal, dodecahedral, octahedral, and cubic

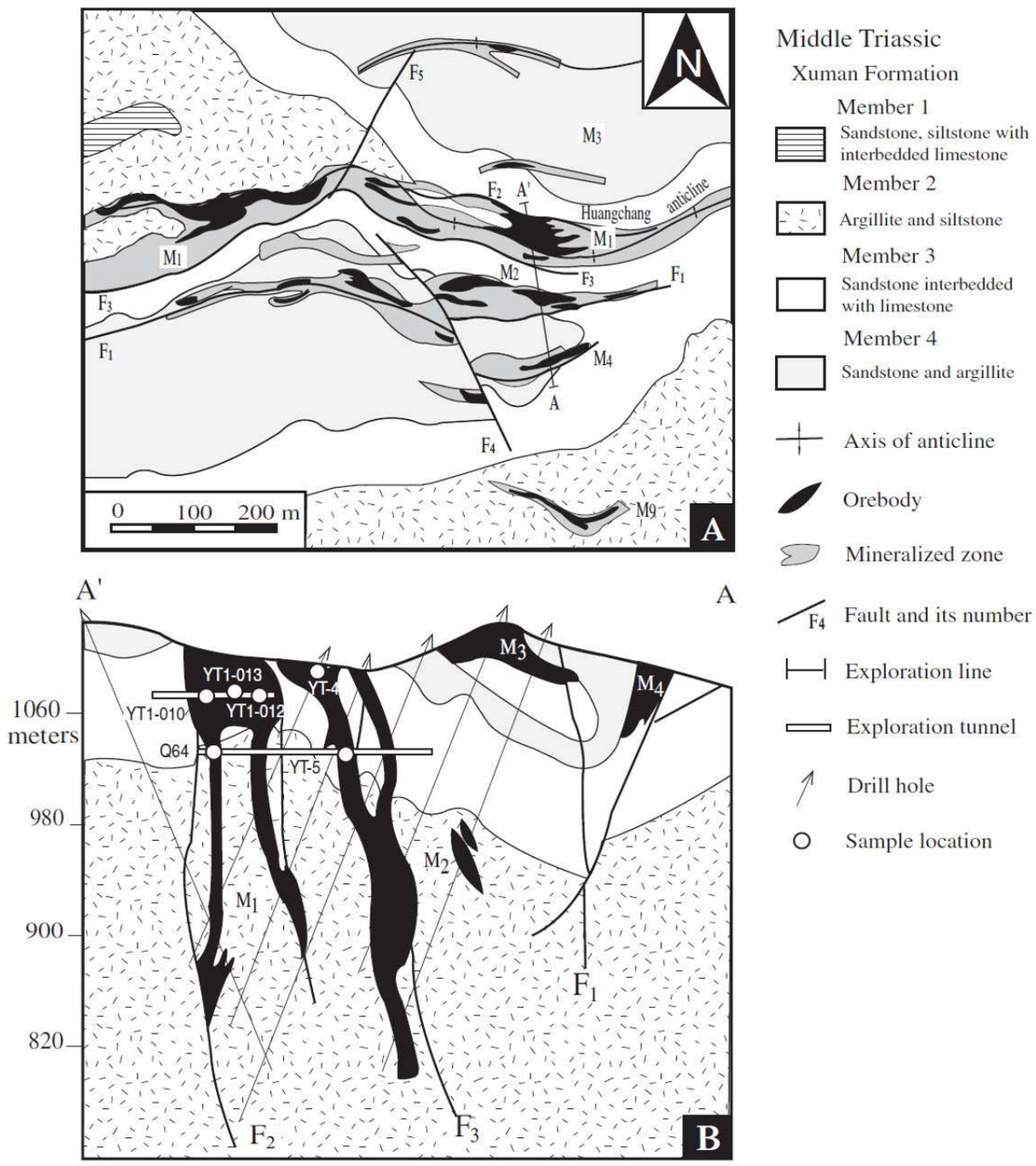

Fig. 4. Simplified geologic plan (A) and cross section (B) along the A-A' exploration line of Yata (after Zhang et al., 2003). Note the vertical (± fault-controlled) orientation of the orebodies.

crystals, or as aggregates of all morphologies. EMPA showed that gold is predominantly in arsenian pyrite (540 ppm Au, 10.73 wt % As: Ye et al., 1994), but a few gold grains (0.3–0.8 μm) have been observed in arsenian pyrite using scanning electron microscopy (Ye et al., 1994). Arsenopyrite is generally disseminated in the ore as tiny acicular to prismatic crystals. Some arsenopyrite occurs as rims on pyrite. Marcasite occurs as rare, tiny grains surrounding pyrite grains. Some stibnite formed early, although later than the gold-bearing pyrite, because stibnite crystals have overgrown on gold-bearing pyrite crystals at their margins. Most of the stibnite formed euhedral crystals filling fractures on the periphery of gold mineralization, local overgrowths of realgar and orpiment (Fig. 4B). Orpiment and realgar are also commonly observed in open cavities with euhedral quartz crystals (Fig. 4K) and fractures in the ore zones or their vicinities. Some calcite-orpiment-realgar veinlets cut pyrite-arsenopyrite-jasperoidal quartz veinlets.

4. Geochemistry of elements and isotope

4.1 Geochemistry of elements

The mineralized rocks in gold deposits in SW Guizhou, are chiefly bioclastic limestone , fine-grained sandstone, siltstone and shale. The gold concentrations are variable for different rock types in different deposits, even within sedimentary rocks of similar type. Generally, siltstones contain higher concentrations of gold than sandstones and shales. As, Sb, Hg, Pb and Zn are generally enriched in weakly mineralized rocks compared to the country rocks in SW Guizhou. However, not only As, Sb and Hg, but also Tl, Mo, and Ag are highly enriched in gold-rich ores compared to the country rocks (Zhang et al., 2003). This phenomenon is particularly noticeable for the ore rocks at Shuiyingdong.

Weakly altered or unaltered samples in Shuiyingdong were selected from various types of rocks for trace element analysis and comparisons were made between their trace element compositions with those of the same type of rocks in the ore-bearing series (Table 1).

As can be seen clearly, the contents of Au, As, Cu, Sb, Tl and Pb in the ore-bearing series are remarkably increased relative to those of unaltered rocks of the same type, reflecting that the trace elements had been brought in by mineralizing hydrothermal solutions. Ti, Sc, Nb, Ta, Zr, Hf, V, Cr, Co, Sn, Ga, Ge, Cd, Rb, Cs, Ba, Mn, Zn, Th and REE showed a little variation in their contents. According to the element geochemical analysis, the former elements belong to the relatively inert elements without having been reworked by hydrothermal solutions, while the latter elements were affected by hydrothermal solutions, slightly influenced by hydrothermal superimposition and reworking processes.

There is no significant difference in primary contents of Au, As, Cu, Sb and Tl for various types of rocks (with unaltered rock samples for reference), and their variation is much less obvious than what was caused by mineralization alteration. As can be seen more clearly from the values of Table 1, the average cotents of Au, As, Cu, Sb and Tl in various types of mineralized rocks are several tens to one hundred times those of the elements in the normal rocks of the same type. Of those elements, the contents of Au, As and Tl are the highest. It may be considered that the contens of these elements in the mineralized rock series were generally affected by mineralizing hydrothermal activities. Relatively speaking, their primary contents in the protoliths can be ignored. These elements are the basic hydrothermal elements in the Shuiyindong gold deposit. Their ratios can be used as the

basic parameters for measuring the hydrothermal alteration intensity. As, Cu, Sb and Tl, especially As, can be employed as the indicator elements for ore exploration.

Element	Average value of ore-bearing rocks/normal rocks				Element	Average value of ore-bearing rocks/normal rocks			
	Limestone	Muddy limestone	Claystone	Muddy siltstone		Limestone	Muddy limestone	Claystone	Muddy siltstone
Au	79.80	55.14	69.33	82.50	Zr	1.15	1.34	1.32	0.70
Sc	1.06	1.14	1.15	0.50	Nb	1.32	1.42	1.29	0.68
TiO_2	1.25	1.04	1.19	0.62	Mo	1.59	6.56	1.42	1.48
V	0.65	1.46	1.23	0.66	Cd	1.87	2.76	2.67	6.31
Cr	0.55	2.32	1.01	0.54	Sn	0.57	2.20	1.79	0.97
MnO	1.25	1.69	0.45	1.20	Sb	2.91	7.95	11.73	32.80
Co	1.30	1.41	1.86	0.62	Cs	1.94	1.39	1.05	0.32
Ni	1.22	1.12	1.06	0.72	Ba	1.01	0.73	1.14	3.07
Cu	3.74	2.27	2.47	1.57	Hf	0.95	1.29	1.29	0.73
Zn	2.07	1.92	1.04	0.82	Ta	1.17	1.29	1.28	0.73
Ga	1.32	1.18	1.38	0.63	Tl	109.0	53.27	69.07	34.92
Ge	0.50	1.17	1.20	0.71	Pb	1.53	1.52	1.62	1.30
As	22.00	19.39	94.26	63.08	Th	0.96	1.04	1.21	0.79
Rb	1.60	1.14	1.51	0.87	U	0.70	3.34	1.47	2.01
Sr	0.25	0.60	0.51	0.86	ree	0.95	1.52	1.42	0.72
Y	0.84	1.61	1.31	0.74					

Table 1. Average values of elements in ore-bearing rock seires and content ratios of elements of normal rocks of the Shuiyindong gold deposit (unit: wt% for TiO_2, MnO, and 10^{-6} for the others).

The result of elements analysis of rocks and ores indicates that the contents of Au, As, Cu, Sb, Tl in rocks are similar and original differences of their contents in rocks is much smaller than the differences caused by hydrothermal alteration. The average contents of these elements in mineralized rocks are tens times even hundred times higher than nonmineralized rocks. So, the contents of these elements are controlled by action of ore-forming fluids. These elements are most basic elements representing action of ore-forming fluids and indicator elements of prospecting.

4.2 Stable Isotopes

The sulfur isotopic composition of pyrite in the ore varies significantly, with $\delta^{34}S$ values varying within the range of +27.17‰– -8.64‰, with a range value of 35.81‰, indicanting a high measure of dispersion. There would be shown the characteristics of sulfur of sedimentary origin and the involvement of other sources of sulfur. Electron microscopic analysis of pyrite monomineral (Fig. 5) indicated that pyrite in the ore contains fram-boid (irregular) pyrite powder crystals and zonal pyrite with arsenopyrite surface (hydrotheral origin) and framboid (irregular) pyrite core (primary sedimentary origin). The sulfur isotope values can only represent those of pyrite of primary sedimentary origin and hydrothermal origin. In most cases the volume of pyrite inner core (petrogenesis) is much larger than that of the girdles of arsenopyrite formed during the metallogenic period. Therefore, the sulfur isotope values obtained mainly represent the sulfur isotopic composition of pyrite of petrogenic origin, but can not fully represent the sulfur isotopic composition of ore-forming fluids (Zhang et al., 2010).

However, the $\delta^{34}S$ values of realgar range from 0.81‰ to 3.03‰ and close to the value of mantle with the range 2.22‰, mean value 1.6‰, indistinctive variation and high homogenization, indicating that the ore-forming substance was probably derived mainly from the deep place (Zhang et al., 2010).

The $\delta^{13}C_{V\text{-}PDB}$ values of calcite which is the main gangue mineral vary from -8.473～0.866‰, with two main distribution from -4～-9‰ and around 0‰. According to the previous literatures, carbon derived from the mantle and the formation (Zhang et al., 2010).

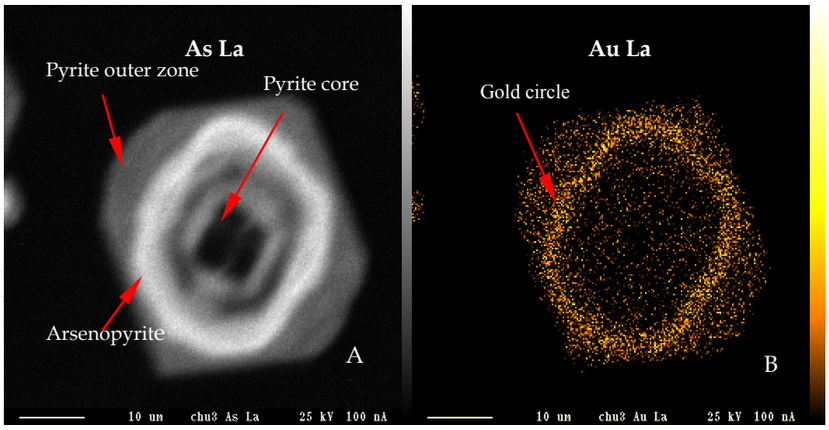

Fig. 5. Scan images of As La(A) and Au La(B) compositions of fine-grained pyrite by electron microprobe spectral scaning.

5. The Sm-Nd isotopic composition of the Shuiyindong gold deposit and its ore-forming geochronological study

In the Carlin-type gold deposits there are usually no minerals suitable for traditional dating, so the problem of metallogenic time has not yet been solved. In the past the fission track method, the quartz fluid inclusion Rb-Sr method and the pyrite Pb-Pb method were used to

constrain the metallogenic ages, giving a larger age range of 80–170 Ma (Hu et al., 2002). Studies by researchers from the Institute of Ore Deposits Geology showed that there are usually developed carbonate veins or realgar (orpiment)-stibnite-carbonate veins in the fault zones exposed on the surface or the hanging-wall of orebodies in the Carlin-type gold mining districts of SW Guizhou. The extensive development of such carbonate veins may imply that there had occurred such geochemical processes as interactions between Au-bearing hydrothermal solutions and Fe-bearing carbonate strata or cements (decarbonation) and they would be the most direct macroscopic geological manifestion of decarbonation during gold metallogenesis.

REE analyses indicated that there are significant differences between the calcite veins closely associated with gold metallogenesis and those with no connection with gold metallogenesis on a regional scale (Table 2, Figs. 6 and 7). The analytical results of Sm-Nd isotopic composition for calcite veins which have close genetic connections with gold mineralization are listied in Table 4 and the calculated results of Sm-Nd isotopic ages are shown in Fig.8. All the results showed that the considerably reliable mineralization age of the super-large Shuiyindong strata-bound Carlin-type gold deposit is 134–136 Ma (Early Cretaceous), just corresponding to the tectonic background of the regional lithosphere expansion(Su Wenchao et al., 2009).

Sample No.	La	Ce	Pr	Nd	Sm	Eu	Gd	Tb	Dy	Ho	Er	Tm	Yb	Lu
Cal-08	0.43	1.77	0.45	3.33	2.38	1.08	3.99	0.7	3.07	0.49	1.05	0.1	0.57	0.07
Cal-11	0.73	3.08	0.73	5.58	3.82	1.89	5.85	0.96	4.32	0.65	1.3	0.14	0.72	0.09
Cal-16	0.18	0.68	0.15	1.05	0.48	0.19	0.57	0.1	0.44	0.08	0.21	0.02	0.14	0.02
Cal-03	6.54	17.1	3.1	16.06	3.81	1.87	3.46	0.46	1.96	0.3	0.61	0.06	0.29	0.04
Cal-17	0.63	2.1	0.4	2.4	0.95	0.41	1.51	0.26	1	0.14	0.22	0.02	0.12	0.02
Cal-10	0.64	1.58	0.38	2.26	0.85	0.28	1.2	0.2	1.02	0.2	0.5	0.05	0.31	0.04
Cal-05	1.66	3.96	0.71	3.5	0.85	0.6	0.95	0.12	0.51	0.09	0.21	0.02	0.1	0.01
Cal-20	1.28	4.18	0.67	3.4	1.04	0.34	1.06	0.18	0.75	0.13	0.3	0.04	0.21	0.03
Cal-21	0.99	3.46	0.59	3.16	1	0.37	1.16	0.18	0.89	0.15	0.35	0.04	0.23	0.03
Cal-12	0.09	0.32	0.07	0.46	0.22	0.09	0.32	0.06	0.29	0.05	0.12	0.01	0.07	0.01
Cal-14	0.67	0.25	0.2	0.99	0.21	0.07	0.24	0.03	0.16	0.03	0.07	0.01	0.05	0.01
ZK1648-14	0.45	0.89	0.17	0.95	0.3	0.12	0.46	0.08	0.36	0.07	0.14	0.02	0.09	0.01
ZK3101-22	0.17	0.55	0.12	0.81	0.81	0.17	0.43	0.07	0.31	0.05	0.1	0.01	0.05	0.01
ZK2002-31	0.21	0.7	0.16	1.23	0.32	0.47	2.72	0.64	3.37	0.55	1.02	0.09	0.47	0.07
NN-03	2.06	3.1	0.49	2.357	0.565	0.182	0.961	0.171	1.009	0.221	0.609	0.085	0.5	0.074
NN-04	0.63	1.26	0.22	1.13	0.339	0.0178	0.45	0.064	0.361	0.068	0.149	0.018	0.087	0.011
NN-05-1	2.3	4.41	0.71	3.368	0.795	0.227	1.018	0.18	0.971	0.203	0.569	0.078	0.449	0.071
NN-05-2	1.49	2.47	0.34	1.234	0.2	0.046	0.192	0.032	0.189	0.036	0.103	0.015	0.087	0.013

Table 2. REE data ($\times 10^{-6}$) for calcite samples in the orebodies and wall rocks of the Shuiyindong gold deposit.

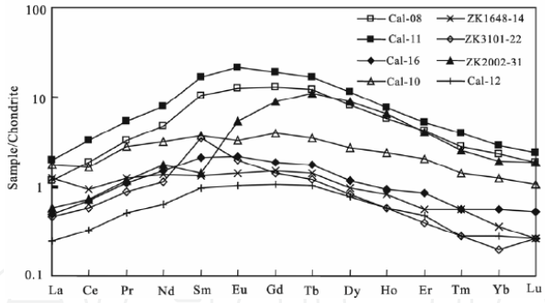

Fig. 6. The chondrite-normalized REE patterns for the calcite veins associated with Au mineralization in the Shuiyindong gold deposit. All data are normalized according to the chondrite REE values of Sun and McDonough (1989).

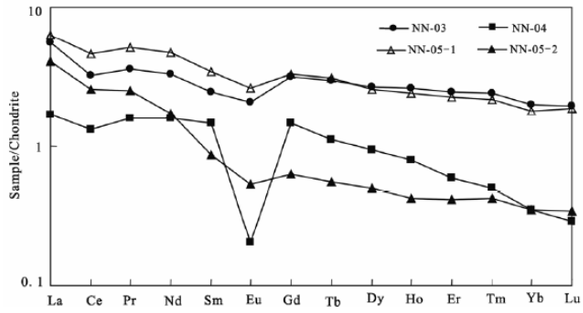

Fig. 7. The chondrite-normalized REE patterns for the calcite veins which have no genetic connection with gold mineralization. All the data are normalized according to the chondrite REE values of Sun and McDonough (1989).

Sample No.	Sm ($\times10^{-6}$)	Nd ($\times10^{-6}$)	$^{147}Sm/^{144}Nd$ (atomic)	$^{143}Nd/^{144}Nd(2\sigma)$ (atomic)	$^{87}Sr/^{86}Sr(2\sigma)$
Cal-08	2.3002	3.0752	0.4522	0.512762±6	0.707083±10
Cal-11	3.8689	5.5334	0.4227	0.512735±5	0.707203±21
Cal-16	0.4683	1.0775	0.2628	0.512593±9	0.707482±13
Cal-03	3.6978	14.5286	0.1539	0.512496±7	0.707251±25
Cal-17	0.9178	2.2416	0.2475	0.512579±6	0.707991±11
Cal-10	0.8437	2.1825	0.2337	0.512567±8	0.707217±13
Cal-05	0.8203	3.2117	0.1544	0.512497±8	0.707152±16
Cal-20	0.9776	3.2226	0.1834	0.512523±12	0.707125±13
Cal-21	0.9602	2.8964	0.2004	0.512537±7	0.707143±10
Cal-12	0.2227	0.457	0.2946	0.512064±6	0.707729±8
Cal-14	0.2044	0.9306	0.1328	0.511922±15	0.707614±10
ZK1648-14	0.2869	0.8801	0.1971	0.511978±20	0.708003±24
ZK3101-22	0.812	0.9904	0.4957	0.512241±18	0.707610±11
ZK2002-31	0.39	0.9459	0.2493	0.512024±7	0.706620±18

Table 3. Sm, Nd and Sr isotopic compositions of calcite veins from the Shuiyindong gold deposit.

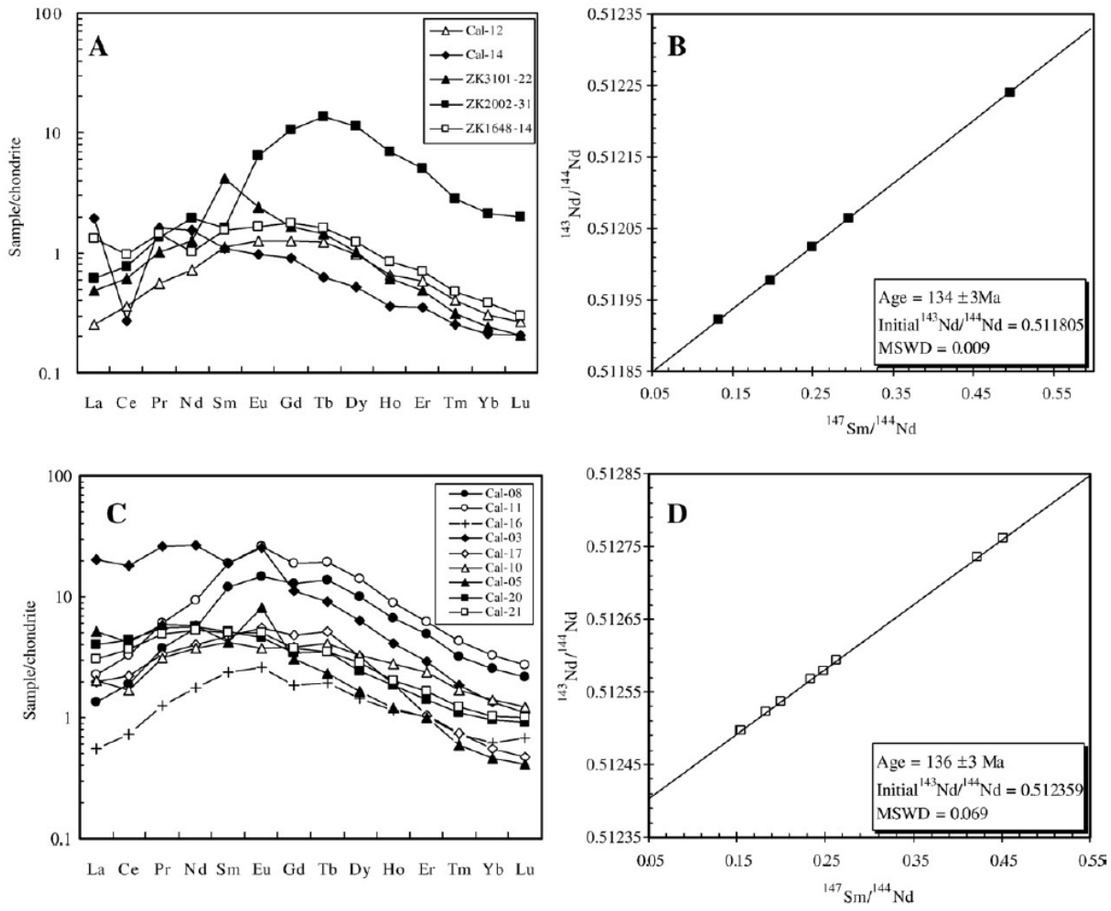

Fig. 8. The chondrite-normalized REE patterns (A and C) and corresponding Sm-Nd isochron ages (B and D) for the calcite veins from the Shuiyindong deposit. All data are normalized using the chondrite REE values of Herrmann (1970).

6. Geochemistry of fluid inclusions

6.1 Fluid inclusion types and petrographic relationships

Eight samples used in this study were collected from the main orebodies in the Shuiyindong and Yata deposits (Figs.3B, 4B). Three are barren milky quartz veins that have early horizontal dips in the ore zones at Shuiyindong and fill fractures at Yata. Some of the milky quartz veins are colored orange or gray by inclusions of realgar or stibnite or are cut by stibnite-realgar-orpiment-quartz veinlets. A sample (YT-5) from Yata contains arsenian pyrite, arsenopyrite, and quartz; other samples from Yata contain stibnite, realgar, orpiment, calcite, and quartz, filling in fractures on the periphery of gold mineralization.

Fluid inclusions observed in this study have negative crystal, elongate, or irregular shapes (Fig. 9). Fluid inclusions types were classified based on their appearance at 25°C andby their Raman spectra and occur in successive stages of the vein and alteration paragenesis.

Type Ia inclusions are two-phase, liquid-rich aqueous inclusions with 10 to 20 vol percent of a low-density vapor bubble at room temperature. They occur in early barren milky quartz veins at Shuiyindong and Yata. Primary inclusions of this type occur along growth zones of quartz and have negative crystal shapes, generally less than 25 μm in diameter (Fig. 9B, E). Secondary inclusions are elongate or irregular and occur along trails crosscutting quartz grains or grain boundaries (Fig. 9C, F). Raman spectroscopy analysis has failed to accurately determine the composition of the vapor phase of this type of inclusion because the bubble moved as the laser beam was focused on it. Raman peaks of CO_2, N_2, and CH_4 have, however, been detected.

Type Ib inclusions are two- or three-phase aqueous-carbonic inclusions with a dominant aqueous liquid phase and a relatively constant carbonic (vapor + CO_2 liquid) fraction of 15 vol percent (Fig. 9H). They are commonly observed in quartz veinlets with arsenian pyrite and arsenopyrite of the main stage of gold mineralization at Yata and in jasperoidal quartz of the main stage at Shuiyindong. Primary inclusions are typically 20μm in diameter, occur along growth zones of quartz, and have negative crystal shapes (Fig. 9G, H). Some inclusions along microfracture planes within quartz grains are pseudosecondary based on their spatial relationship to the growth zones and healed fractures. Both microthermometry and Raman spectroscopy analyses have revealed that the main component of the volatile phase of the inclusions is CO_2, with minor N_2 and trace CH_4.

Type II inclusions are rare, two-phase, aqueous-carbonic inclusions with variably high proportions of a carbonic phase ranging from 45 to 90 vol percent (Fig. 9K). In samples from Yata, they occur in late drusy quartz with realgar, stibnite, and calcite.

Type III inclusions are monophase carbonic inclusions (Fig. 9L) and generally less than 15 μm in diameter. They are restricted to late quartz-realgar veins or veinlets at Yata and occur along trails crosscutting quartz grains. Both microthermometry and Raman spectroscopy have revealed that the volatile phase is mainly composed of CO_2 and N_2, with trace CH_4. Petrographic relationships indicate that CO_2-poor aqueous inclusions of type Ia can be interpreted to approximate the mineralizing fluid, which was responsible for precipitation of early ore minerals in veins but predates the deposition of the bulk of disseminated gold-bearing arsenian pyrite and arsenopyrite deposition in both deposits. CO_2-rich fluids of type Ib are interpreted to correspond to the main gold-bearing fluid in both deposits. The same aqueous-carbonic fluids also occur together with type II and III carbonic fluids in the late quartz-realgar veins at Yata. Type II and III fluids are interpreted to represent the waning or outflow stage of economic gold mineralization.

6.2 Quantitative fluid inclusion results

6.2.1 Microthermometry and Raman data

Microthermometric measurements were made on primary, pseudosecondary, and secondary inclusions in quartz crystals from milky quartz veins, replacement-style quartz veinlets, and late drusy quartz. Three distinctive fluid compositions are interpreted to be

representative of the different mineralization stages. Microthermometric data and Raman spectroscopy analyses of representative fluid inclusions are given in Table4.

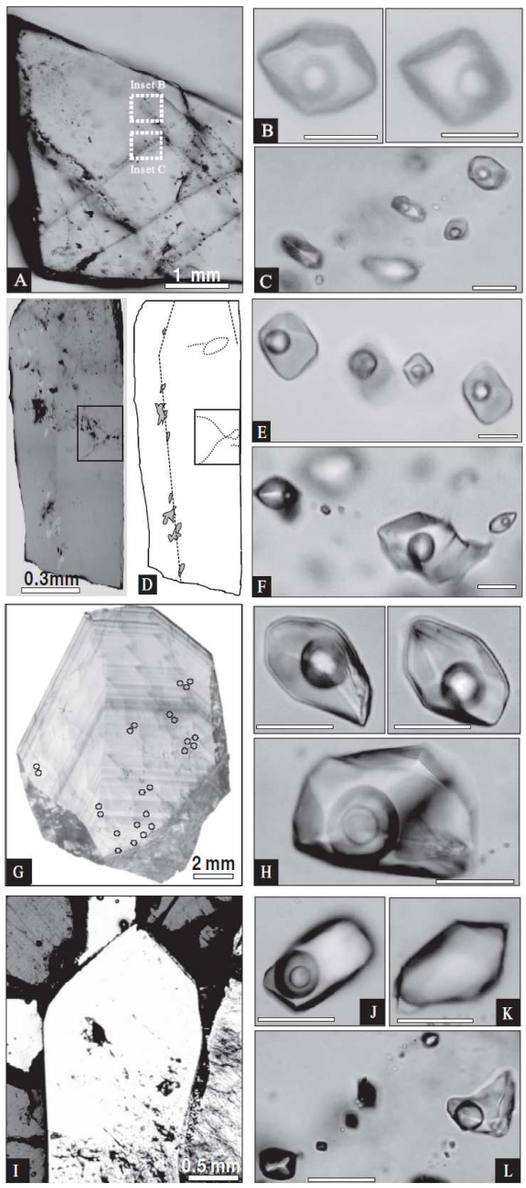

Fig. 9. Microphotographs of fluid inclusions in quartz. A. Early milky quartz (thin section) from Shuiyindong. B. Primary and C. Secondary type Ia aqueous inclusions in the milky quartz from Shuiyindong. D. Photograph and sketch of early milky quartz from Yata. E. Primary and F. Secondary type Ia aqueous inclusions in the milky quartz from Yata. G. SEM-CL image of a main ore-stage quartz crystal, and H. Photographs of type Ib aqueous-carbonic inclusions from Yata. Circles denote the positions of inclusions analyzed by LA-ICP-MS. I. to L. Late drusy quartz crystal with types Ib, II, and III aqueous-carbonic and carbonic-rich inclusions from Yata, respectively. Note that two end-member fluid inclusion assemblages are cogenetic in (L). Scale bar is 20 μm unless defined otherwise.

Stage	Quartz type	Inclusion	Microthermometry						Raman data		
			Tm (CO_2) (^oC)	Th(CO_2) (^oC)	Mode	Tm(cl) (^oC)	Th (^oC)	Mode	CO_2	N_2	CH_4
Main-stage	Veinlet quartz crystals	41	–56.7	20.5	L	9.4	228	L	97.5	1.5	1.0
		42	–57.7	17.6	L	9.3	227	L	95.7	3.3	1.0
		55	–56.7	21.6	L	9.4	220	L	97.0	3.0	n.d.
		60	–56.8	22.2	L	8.8	215	L	96.8	2.0	1.2
		61	–56.6	22.9	L	9.4	210	L	99.5	0.5	n.d.
		65	–56.9	21.4	L		238	L	96.0	3.5	0.5
		66	–56.8	22.3	L		217	L	97.0	3.0	n.d.
		76	–56.7	23.4	L	9.6	223	L	96.8	2.5	0.7
		80	–56.7	23.3	L		206	L	98.2	1.8	n.d.
		93	–56.6	24.8	L	8.6	225	L	98.7	1.3	n.d.
		94	–56.7	24.5	L	9.4	210	L	97.5	1.8	0.7
		99	–56.7	17.9	L	9.0	247	L	96.5	2.7	0.8
		107	–56.7	20.8	L	9.8	216	L	97.2	1.9	0.9
Late stage	Veinlet quartz crystals	34	–58.7	6.3	L	9.5	232[1]		86.5	13.5	n.d.
		35	–58.6	7.8	L	9.3	228[1]		89.2	10.0	0.8
		11	–60.5	–24.3	L				71.0	27.2	1.8
		12	–60.3	–24.0	L				73.0	27.0	n.d.
		14	–60.2	–23.3	L				75.0	25.0	n.d.
		15	–60.2	–23.2	L				77.0	23.0	n.d.

(Notes: Tm (CO_2) = final melting temperature of CO_2, Th(CO_2) = homogenization temperature of CO_2, Tm = melting temperature of ice, Tm(cl) = final melting temperature of clathrate, Th = homogenization temperature; L = homogenize to liquid; [1] Decrepitation temperature; n.d. = not detected; Composition is given in mol percent)

Table 4. Chemical Compositions of Representive Aqueous–Carbonic and Carbonic–Rich Inclusions Obtained by Raman Spectroscopic Analysis and Corresponding Microthermometric Data from Yata.

Type Ia primary and secondary aqueous inclusions (Fig.9B-C, E-F) have initial ice-melting temperatures (Te) from –22.2° to –21.0°C, which is similar to the eutectic melting temperature in the NaCl-H_2O system (Hall et al., 1988) but does not exclude more complex systems such as the NaCl-KCl-H_2O system (Sterner et al., 1988). Final ice-melting temperatures (Tm) of primary aqueous inclusions range from –3.0° to –4.3°C, corresponding to salinities of 5.0 to 6.9 wt percent NaCl equiv (Bodnar, 1993) with an average of 6.0 wt percent NaCl equiv (Fig. 10B, D). Homogenization of these fluid inclusions was to the liquid phase at temperatures ranging from 190° to 258°C with a mode around 230°C (Fig. 10A, C). The Tm of secondary inclusions range from –1.2° to –4.5°C, corresponding to salinities of 2.1 to 7.2 wt percent NaCl equiv (Fig. 10B, D). Secondary inclusions of type Ia also homogenized into the liquid phase at temperatures ranging from 151° to 261°C with a mode around 190°C (Fig. 10C). No evidence of other phases, such as clathrate, liquid, or solid CO_2 were observed, suggesting that this type of inclusion may contain as much as 2.4 mol percent CO_2 dissolved in the aqueous phase without developing a separate CO_2 liquid phase at room temperature (Bodnar et al., 1985).

Type Ib primary and secondary aqueous-carbonic inclusions (Fig. 9H, J) always develop a vapor phase in the carbonic bubble, even if they are two-phase at room temperature. The melting temperature of CO_2 (Tm (CO_2)) ranges from –58.1° to –56.6°C with the majority of

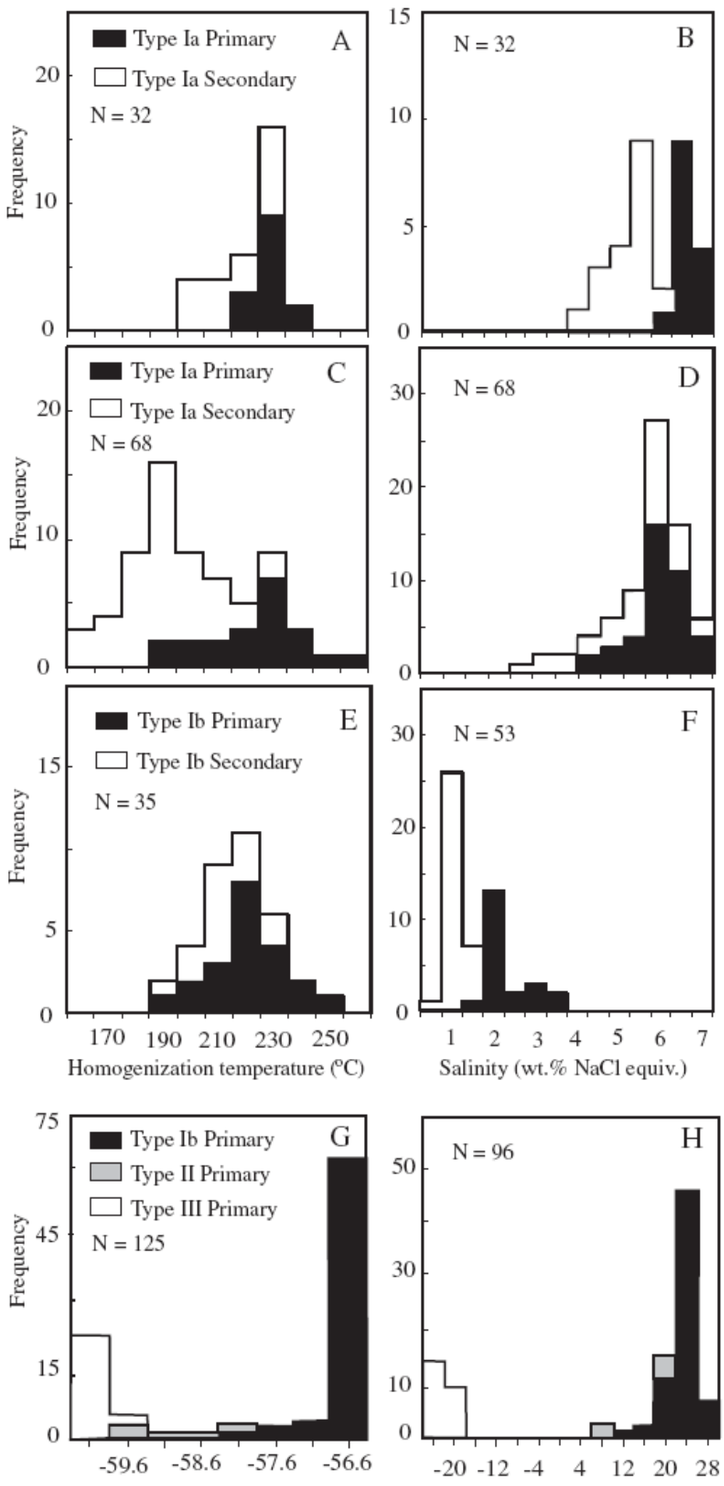

Fig. 10. Histogram of homogenization temperature, final CO_2 melting temperature, and salinity of fluid inclusions from Shuiyindong (A-B) and Yata (C-H).

CO2 melting occurring at –56.6°C (Fig. 10G). The carbonic phase always homogenized to the liquid (Th (CO_2)) at temperatures ranging from 10.2° to 26.1°C with a mode around 24.0°C (Fig. 10H). Clathrate observed in these inclusions exhibits a typical Q2 melting behavior (Bakker and Brown, 2003). The clathrate melting temperatures (Tm(cl)) of primary inclusions range from 8.3° to 9.2°C, corresponding to salinities of 1.6 to 3.3 wt percent NaCl equiv (Diamond, 1992), with an average of 2.3 wt percent NaCl equiv (Fig. 10F), which is two to three times lower than the salinity of the type Ia aqueous inclusions. The Tm(cl) of secondary inclusions range from 9.4° to 9.8°C, corresponding to salinities of 0.4 to 1.2 wt percent NaCl equiv (Fig. 10F). These inclusions commonly decrepitated at temperatures below 200°C, before total homogenization was attained.

The 35 inclusions that did not decrepitate homogenized into the liquid phase at temperatures from 190° to 245°C, with a mode around 220°C (Fig. 10E). Raman spectroscopy of the carbonic phase in individual fluid inclusions showed that CO_2 is the dominant volatile (>96 mol %), N_2 is always detected (0.5–3.5 mol %), and CH4 has been detected (up to 1.2 mol%) in a few inclusions (Table 4).

Type II aqueous-carbonic inclusions (Fig. 9K) also always develop a vapor phase in the carbonic bubble during cooling runs. Their Tm(CO2) ranged from –59.6° to –58.1°C (Fig.10G). Homogenization of the CO_2 was always to the liquid phase between 6.3° to 20.9°C. The Tm(cl) range from 9.5° to 10.7°C, corresponding to salinities of 0 to 8.9 wt percent NaCl equiv (Bakker and Brown, 2003). Total homogenization temperatures were not obtained because these inclusions decrepitated when heated to above 200°C. Raman spectroscopy revealed that their volatile phases contain major CO_2 (87–89 mol %), minor N_2 (10–14 mol %), and trace CH_4 (0.8 mol %; Table 4).

In the process of freezing (down to –180°C) and subsequent heating, type III carbonic inclusions (Fig. 9L) underwent the following sequence of phase transitions: S + V → L + V → L. The Tm(CO_2) range from –60.5° to –59.6°C with the majority at –60.1°C (Fig. 10G). The Th(CO_2) of this type of inclusion range from –24.3° to –22.5°C (Fig. 10H) and were always into the liquid phase. Total homogenization temperatures could not be measured reliably owing to optical limitations (Diamond, 2003). Raman spectroscopy showed that the volatile phase of type III inclusions contains major CO_2 (71–77 mol %), minor N_2 (23–27 mol %), and trace CH_4 (up to 1.8 mol %; Table 4).

6.2.2 Bulk compositions of aqueous-carbonic and carbonic-rich fluids

Aqueous-carbonic inclusions in the main stage of pyrite-arsenopyrite-quartz veins and late stage of stibnite-realgar-orpiment-quartz veins at Yata have 10 to 15 vol percent volatile phase (nearly pure CO_2), regardless of the sample localities. Calculated density of the volatile phase varies from 0.72 to 0.82 g/cm3, with an average of 0.75 g/cm^3. Calculated bulk compositions showed that the fluids are dominated by H_2O (91–92 mol %) and CO_2 (6.3–8.4 mol %, with an average of 7.6 mol %). Their bulk densities range from 0.97 to 0.99 g/cm^3. Their average salinities vary from 0.9 to 2.3 wt percent NaCl equiv. Calculated bulk compositions of carbonic-rich inclusions in the late stage of stibnite-realgar-orpiment-quartz veins at Yata are dominantly CO_2 (58–64 mol %), N_2 (19.2–23.7 mol %), and H_2O (12.5–22.8 mol %), and trace CH_4 (up to 1.6 mol %), with volatile phase densities and bulk densities of 0.75 to 0.80 and 0.77 to 0.82 g/cm^3, respectively.

6.3 Pressure and temperature estimation

The compositions of type Ib inclusions plot close to the solvus of the H_2O-CO_2 system at 1.0 kb in Figure 8A. It is possible that the fluids of these inclusions may represent one end member produced by unmixing of H_2O-CO_2 fluids. The compositions of a few type II inclusions plot in the two-phase field in Figure 11A. These inclusions may represent mechanical mixtures of two immiscible fluid phases. The local occurrence of type II inclusions at Yata indicates that the hydrothermal fluid reached a state of immiscibility at some time in its history (Diamond, 1990). Type III inclusions plot close to the 1.0 kb solvus in Figure 8A. If they coexisted with type Ib inclusions, then these inclusions may represent another end member produced by unmixing of H_2O-CO_2 fluids.

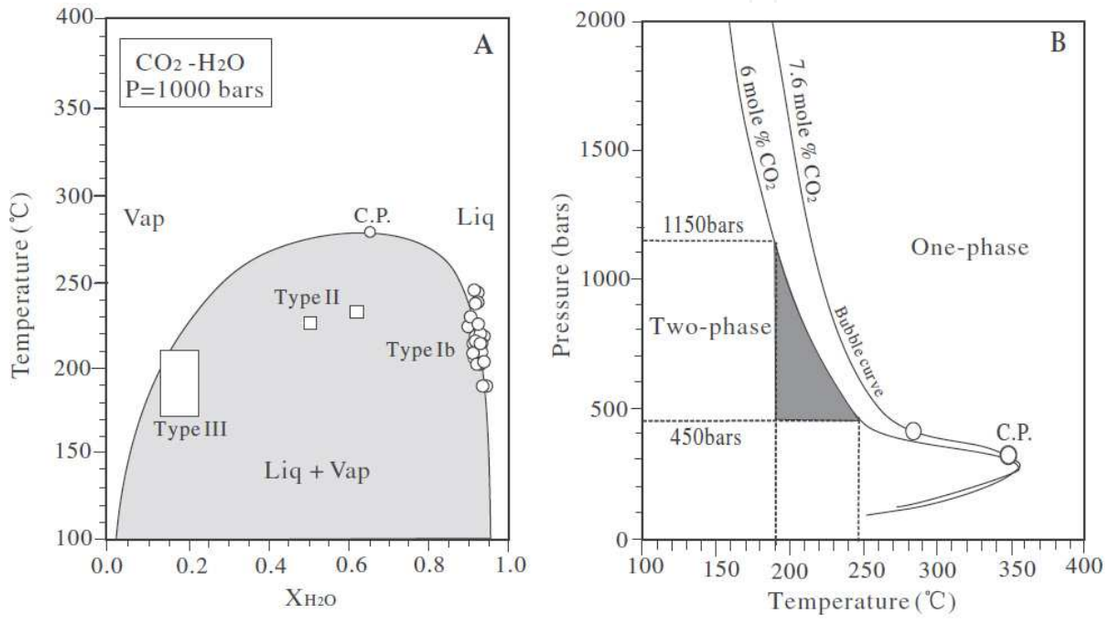

Fig. 11. A. T-X diagram of the H_2O-CO_2 system at 1.0 kbar based on experimental data from Tödheide and Franck (1963)and Takenouchi and Kennedy (1964). B. P-T diagram showing the range of possible P-T conditions during mineralization at Yata. The miscibility boundaries for fluids with 6 and 7.6 mol percent CO_2 are from experimental data of the H_2O-CO_2 system of Tödheide and Franck (1963) and Takenouchi and Kennedy (1964).

The minimum P-T conditions of inclusion entrapment are constrained by intersecting points using the range of homogenization temperatures of type Ib inclusions (190°–245°C) and the minimum of the bubble curves of 6 mol percent CO_2 (Fig. 11B). The defined area in Figure 8B (shaded) ranges from 450 to 1,150 bars, corresponding to a depth of 1.7 to 4.3 km under lithostatic load, using the average density of sedimentary rocks in southwestern Guizhou (2.67 g/cm^3: Wang et al., 1995) and 4.5 to 11.5 km assuming hydrostatic pressure. As Yata was controlled by a fault, the estimated pressure may have been fluctuating between hydrostatic and lithostatic pressures. Decompression associated with episodes of faulting may have caused the immiscibility in the late stage of stibnite-realgar observed in this deposit. Zhang et al. (2003) previously estimated pressures for the Lannigou deposit ranging from 600 to 1,700 bars based on the CO_2-bearing fluid inclusions, corresponding to a depth of 2.2 to 6.3 km under lithostatic conditions or an unlikely 6 to 17 km under hydrostatic

load. CO_2 contents of fluid inclusions at Yata (6–8 mol %) are somewhat lower than those of many orogenic lode gold deposits (10–25 mol % CO_2: Ridley and Diamond, 2000) but higher than those of Carlin-type gold deposits in Nevada (2–4 mol % CO_2: Hofstra and Cline, 2000). It is, therefore, reasonable to infer that the Yata deposit may have formed at depths intermediate between orogenic-type gold deposits and those of the Carlin trend in Nevada.

6.4 Source of fluids

Oxygen and hydrogen isotope compositions of early barren milky quartz veins and clay minerals (<2 μm) in the mineralized rock from Shuiyindong have been reported by Hofstra et al. (2005). The milky quartz veins have a narrow range of high $\delta^{18}O$ values (21–27‰). Calculated $\delta^{18}O(H2O)$ values for fluids in these samples vary from 10.5 to 16.5 per mil, using a homogenization temperature of 230°C from this study and the quartz-water isotopic equilibrium fractionation equation of Friedman and O'Neil (1977). Calculated δ18O(H2O) and δD(H2O) values for fluids in equilibrium with clay minerals in the mineralized rocks at Shuiyindong range from 4 to 10 and –56 to –68 per mil, respectively (Hofstra et al., 2005). Similar fluid calculations for clay minerals in the mineralized rocks from the Zimudang deposit, located 15 km west of Shuiyindong on the same large-scale dome structure, indicate $\delta^{18}O(H_2O)$ and $\delta D(H_2O)$ values from 13 to 16 and –35 to –40 per mil, respectively (Hofstra et al., 2005).

Li et al. (1989) and Zhu et al. (unpub. data) reported oxygen for the main ore quartz and the late ore calcite from Yata. The main ore quartz has a narrow range of $\delta^{18}O$ values (20.9–26.1‰), similar to milky quartz veins at Shuiyindong. The calculated $\delta^{18}O(H_2O)$ values for the main ore fluids from Yata vary from 9.9 to 15.1 per mil at 220°C. The $\delta^{18}O(H_2O)$ values of late ore fluids (8.1–10.9‰) were calculated from measured $\delta^{18}O$ calcite values (18.2–20.8‰), the minimum homogenization temperature of 190°C for CO_2-bearing fluid inclusions within calcite (Zhang et al., 2003) and the calcitewater isotopic equilibrium fractionation equation of Friedman and O'Neil (1977). The δD(H2O) values of water extracted from inclusion fluids in the main ore quartz at Yata range from –51.1 to –78.8 per mil (Li et al., 1989), significantly higher than the average $\delta D(H_2O)$ value of local meteoric water during the Jurassic and Cretaceous (–85‰: Han et al., 1999). The $\delta^{18}O(H_2O)$ and $\delta D(H_2O)$ values plot within or close to the metamorphic-water box (Hofstra et al., 2005, fig. 3), suggesting that the ore fluids are characterized by a predominantly metamorphic component. There is no evidence for meteoric water involvement, but a deep magmatic component cannot be excluded.

6.5 Processes of gold deposition

Recent studies of Carlin-type deposits in Nevada have concluded that gold-rich arsenian pyrite precipitated from H_2S rich fluids, which sulfidized iron-bearing minerals in the host rocks (Hofstra et al., 1991; Hofstra and Cline, 2000). The chemical reaction of cooling H_2S-rich fluids in contact with iron-poor carbonate-bearing sedimentary rocks has been calculated from thermodynamic data by Heinrich (2005). An important prediction is that Au solubility may remain high to temperatures as low as 150°C, provided that an excess of H_2S over Fe is maintained in a moderately oxidized hydrothermal fluid, the pH of which is kept close to neutral by carbonate dissolution (Heinrich, 2005, fig. 6). This fluid-chemical evolution path can equally apply to fluids of magmatic or metamorphic origin but clearly

matches the low Fe contents of fluids measured in the inclusions from the Shuiyindong and Yata deposits. At the strata-bound Shuiyindong deposit, there is no evidence for significant phase separation during the main mineralization stage. At the fault-controlled Yata deposit, phase separation was minor during gold mineralization and common in the late stibnite-realgar stage. This fluid inclusion evidence suggests that phase separation was not the key process for deposition of gold and arsenian pyrite. The low Fe contents in the ore fluids (below 400 μg/g) measured by LA-ICPMS of fluid inclusions and many relict inclusions of ferroan carbonate (with up to 7.0 wt % Fe determined by EMPA: Su et al., 2008) enclosed in the jasperoidal quartz crystals suggest that iron in sulfide minerals was probably derived from dissolution of ferroan carbonate in the host rocks, as has been documented in Carlin-type gold deposits in Nevada by lithogeochemistry of ores (Hofstra et al., 1991; Hofstra and Cline, 2000). Sulfidation of ferroan carbonate-rich host rocks by H2S-rich ore fluids containing $Au(HS)^{-2}$ or $Au(HS)^{0}$ (Seward, 1973, 1991), along with arsenic as H_3AsO_3 (aq) complex (Heinrich and Eadington, 1986; Pokrovski et al., 2002), would have effectively extracted gold from solution and transformed primary ferroan carbonate to secondary gold-bearing arsenian pyrite, possibly by a coupled reaction such as the following:

$$2FeCO_3 + 2H_3AsO_3\ (aq) + H_2S(aq) + 2Au(HS)_2^{-}(aq) + H_2\ (g)$$

$$= Fe(S, As)_2 \cdot Au_2S^0 + FeS_2 + CO^{-2}_3(aq) + CO_2\ (g) + 7H_2O.$$

Any loss of CO_2 by fluid phase separation would further promote the formation of gold-bearing arsenian pyrite by such a reaction. This is consistent with petrographic observations that gold-bearing arsenian pyrite and arsenopyrite occur together with Fe-poor hydrothermal dolomite (Fig. 4C). Moreover, it can explain the covariance of Au, As, Sb, and Sr contents of the ore fluids (Fig. 9). The reaction involves reduction of As (+III) and Au (+I) by consumption of H_2 (g), which can be provided by reaction of the metal-transporting fluids with the local organic-rich sediments. This situation is likely to occur where fluids are channeled into a fluid conduit (e.g., along the unconformity between the Maokou Limestone and the Longtan Formation at Shuiyindong or the reverse faults at Yata). Here, they reacted with carbonaceous and Fe carbonate-rich host rock, or were mixed with Fe+2- and CH4-bearing pore fluids previously equilibrated with the reduced host-rock package, to deposit arsenian pyrite and arsenopyrite that host most of the gold in the deposits. The generation of secondary pervasive permeability and porosity by carbonate dissolution from the host rocks favors fluid focusing and the formation of strata-bound orebodies (Heinrich, 2005), as is the case in the Shuiyindong. Therefore, fluid reduction and sulfidation of wall-rock iron by H_2S-rich ore fluids are proposed to be the most important mechanism of gold deposition as auriferous arsenian pyrite in the Chinese Carlin-type gold deposits.

Genetic models previously proposed for Carlin-type deposits in Nevada fall into three groups involving magmatic (Radtke et al., 1980; Ressel et al., 2000), metamorphic (Groves et al., 1998; Hofstra and Cline, 2000), and deeply or shallowly circulated meteoric waters (Ilchik and Barton, 1997; Emsbo et al., 2003). Our study of Carlin-type deposits in Guizhou indicates that the ore fluids are of low salinity but rich in highdensity CO_2, and stable isotope data are consistent with a dominant metamorphic fluid source. The ore-forming fluids have extremely high contents of the characteristic ore elements (As, Sb, and Au), and the mineralogical characteristics and high gold grade of the deposits can be explained by interaction of such fluids with chemically reactive carbonate-, iron-, and carbon-rich

sedimentary host rocks. The deposits formed at similar temperatures as epithermal gold deposits, but at significantly higher pressure and greater depths (4–6 km), consistent with regional-metamorphic temperature gradients. Their thermal regime and ore fluid characteristics are similar to those of the broad group of orogenic gold deposits, raising the possibility that the Carlin-type deposits in Guizhou might be the basin-hosted and relatively cool end member of the crustal continuum of orogenic gold deposit formed from fluids liberated by deep metamorphic dehydration or magmatism (Groves, 1993; Groves et al., 1998; Pettke et al., 2000).

7. Metallogenic model

Through comprehensive geological-geochemical studies and discusion on the problems concerning metallogenesis, the metallogenic model of the Shuiyindong gold deposit can be summarized as follows(Xia 2005; Zhang et al., 2010):

Late Indosinian to Early Yanshanian tectonic movements put the end to the history of basin evolution in this region. Development of strata folds, faults, deep giant faults and magmatism, abnormally high geothermal temperature, and deeper burial resulted in the formation of ore fluids with abundant volatile elements in the deep interior of the crust and upper mantle. In addition, the fluids also became the overpressured fluids after extracting ore-forming elemens in the Au-, Hg-, Sb-, As- and Tl-rich rocks in the basement and at great depth.

At that time, as the crust was in the compressive sealed stress state, the overpressured ore fluids were sealed at depth and were in strong equilibrium with the lithosphere. During the Yanshanian period this region was in the extensional state. With the injection of alkaline ultrabasic dykes (tubes), resurvival of the faults had occurred at the basement, which, together with cover-strata faults, cut through the crust. As a result, the sealing conditions of overpressured ore fluids were destroyed, the fault system, like a pump, made ore fluids find their way into the upper crust. Gold in the ore fluids would be rapidly precipitated and accumulated as gold deposits in the favorable loci where metallogenic conditions changed suddenly. Meanwhile, Hg, Sb, As, Tl and other ore-forming elements would be precipitated as ores in the proper locations. All these led to what we see today in Southwest Guizhou, where the Carlin-type gold deposits are characterized by close Au-Hg-Sb-As-Tl paragenesis or association on a regional scale, while various gold deposits show the phenomenon of differentiation. At that time, as for the Shuiyindong gold deposit, due to the formation of the Huijiabao short-axis anticline and that of the favorable Upper Permian Longtan Formation assemblage of claystone→bioclastic limestone→claystone, volatiles with abundant CH4, N2 and CO2, which found their way into the anticline core along the karst and non-kart unconformability at the bottom of the Longtan Formation, and gold overpressured ore fluids were gathered. The fluids contained no iron (Su Wenchao et al., 2006), gold can be exist in the form of Au-S coordination compound (Seward, 1973; Hofstra and Cline, 2000; Zhang Jun et al., 2002). Relatively high pressure and high volatiles made ore fluids move laterally and infiltrate to some extent in bioclasstic sandy limestones in the favorable lithologic assemblage. Sometimes, the overpressured ore fluids would hydrodynamically destroy the country rocks. With the structural development, the faults destroyed the traps constituted by the anticline and favorable lithologic assemblage, making volatiles in the fluids escape out rapidly. As a result, the fluid pressure dropped suddenly, followed by the

decrease of reductivity and the local or partial involvement of iron, some other components and meteoric water in the strata, leading to significant differences in ore-forming conditions. The ore-forming conditions thus rapidly turned favorable for gold deposition, and gold would be rapidly precipitated with the crystallization of arsenopyrite (partly in the inner core of pyrite of sedimentary origin) or fine-grained cinnaba.

Run-through of the faults and the repeated occurrence of favorable lithologic assemblages led to the multi-layer orebody occurrence of the Shuiyindong gold deposit (Fig. 14). And Hg and Tl in metallogenic hydrothermal solutions possess much higher mobility, thus forming ore deposits in high-angle tensional-shear faults in the priphery of the gold deposit. Therefore, there appeared anticline core and low-angle compresso-shear fault strata-bound gold deposits and slightly later high-angle tensional-shear strata-bound Hg and Hg-Tl deposits.

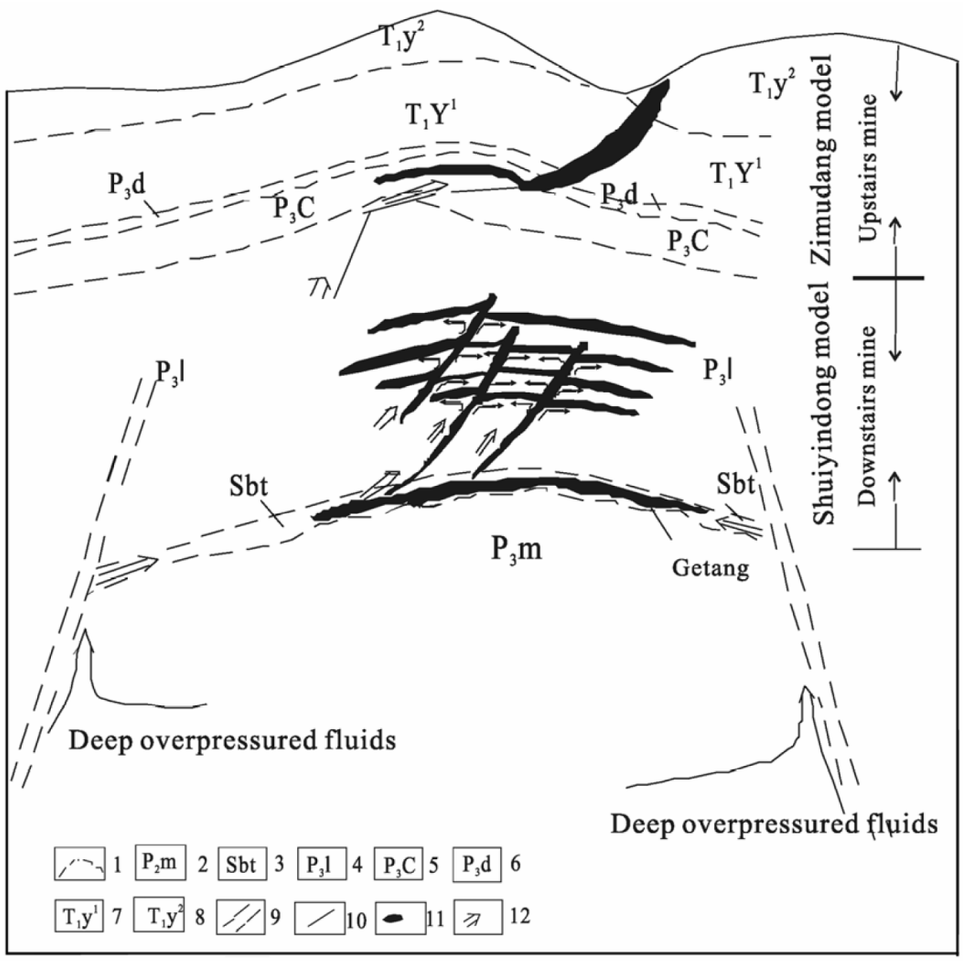

Fig. 11. The ''two-stories'' gold orebodies distribution and metallogenic model of the Carlin-type gold deposit in SW Guizhou (after Xia, 2005). 1. Stratum boundary; 2. Maokou Formation; 3. alteration zone; 4. Longtan Formation; 5. Changxin Formation; 6. Dalong Formation; 7. the first member of the Yelang Formation; 8. the second member of the Yelang Formation; 9. deep giant fault; 10. fault; 11. gold orebody; 12. migration direction of ore-forming fluid.

Studies showed (Su Wenchao et al., 2006) that the mineralization experienced decarbonation, gold and sulfur precipitation and the formation of carbonate veins, The chemical reactions involved in these three processes are presented as follows:

1. Decarbonation:

$$CO_2+H_2O=H_2CO_3 \quad (1)$$

$$H_2CO_3+(Ca, Fe)CO_3=Fe^{2+}+Ca^{2+}+2\,HCO_3^- \quad (2)$$

2. Precipitation of gold and sulfides:

$$Au(HS)_2^-+0.5\,H_2=Au^0+H_2S+HS^- \quad (3)$$

$$2H_2S+Fe^{2+}=FeS_2+2H^++H_2 \quad (4)$$

3. Formation of carbonate veins:

$$2HS^-+Fe^{2+}=FeS_2+2H^+ \quad (5)$$

$$Ca^{2+}+CO_3^{2-}=CaCO_3 \quad (6)$$

a. Weak acidity of Au-bearing hydrothermal solutions made Fe-carbonate minerals in ore-hosted wall rocks dissolve, followed by the release of Fe and Ca into the hydrothermal system [Reactions (1) and (2)], i.e., decarbonation. b. $Au(HS)^{2-}$ in hydrothermal solutions was decomposed under relatively reducing conditions, making H_2S and HS^- enter into the hydrothermal system [Reaction (3)], both of them together with Fe-carbonate minerals were dissolved, releasing Fe^{2+}-bound pyrite (sulfidation) and producing H^+ [Reactions (4) and (5)].

The acidic environment resultant from sulfidation may further promote Fe-carbonate minerals in the wall rocks to dissolve, followed by the release of a large amount of Fe^{2+} into the hydrothermal system. Sulfidation would finally lead to the over-saturation of Au in hydrothermal solutions and its precipitation as native gold grains and accumulation on the surface of arsenopyrite grains or their margins. c. Dissolution of Fe-carbonate minerals led to the release of Ca [Reaction (6)], which would be involved in the formation of late calcite veins, accompanied by Au pyrite veinlets or cutting through the latter. Therefore, high-grade Fe-carbonate ore-hosted wall rocks are one of the important factors for the formation of large-sized Carlin-type gold deposits. Carbonate veins associated with decarbonation may be one of the important indicators for search of large-sized Carlin-type gold deposits.

8. Acknowledgments

The project was supported jointly by the State Science and Technology Supporting Program (2006BAB01A13), the self-research project funded by the State Key Laboratory of Ore Deposit Geochemistry (Ore Deposit Special Research Project), and Guizhou Provincial Bureau of Geology and Mineral Resource Exploration and Development [Qian Di Kuang Ke (2009) No. 11].

9. References

Bakker, R.J. & Brown, P.E. (2003). Computer modelling in fluid inclusion research, Mineralogical Association of Canada Short Course Series, Vol. 32, pp. 175-212

Bodnar, R.J. (1993) Revised equation and table for determining the freezing point depression of H2O-NaCl solutions. Geochimica et Cosmochimica Acta, Vol. 57, (February 1993), pp. 683-684, ISSN 0016-7037

Bodnar, R.J., Reynolds, T.J. & Kuehn, C.A. (1985). Fluid inclusion systematics in epithermal systems. Reviews in Economic Geology, Vol. 2, pp. 73-79, ISSN 0741-0123

Bureau of Geology and Mineral Resources of Guizhou Province (1987), Regional Geology of Guizhou Province: Geological Memoirs S.1, No. 7, pp. 1-698, Geological Publishing House Beijing(in Chinese)

Diamond, L.W. (1990). Fluid inclusion evidence for P-V-T-X evolution of hydrothermal solutions in late-alpine gold-quartz veins at Brusson, Val D'Ayas, northwest Italian Alps. American Journal of Science, Vol. 290, (October 1990), pp. 912-958, ISSN 0002-9599

Diamond, L.W. (1992). Stability of CO2 clathrate + CO2 liquid + CO2 vapour + aqueous KCl-NaCl solutions: Experimental determination and application to salinity estimates of fluid inclusions. Geochimica et Cosmochimica Acta, Vol. 56,No. 1,(January 1992), pp. 273–280, ISSN 0016-7037

Diamond, L.W. (2003). Introduction to gas-bearing aqueous fluid inclusions: Mineralogical. Association of Canada Short Course Series, Vol. 32, No. 1-8, pp. 101-158

Emsbo, P., Hofstra, A.H., Lauha, E.A., Griffin, G.L. & Hutchinson, R.W. (2003). Origin of highgrade gold ore, source of ore fluid components and genesis of the Meikle and neighboring Carlin-type deposits, north CarlinTrend, Nevada. Economic Geology，Vol. 98, (September 2003), pp. 1069-1105, ISSN 0361-0128

Friedman, I. & O'Neil, J.R. (1977). Compilation of stable isotope fractionation factors of geochemical interest, U.S.G.S. Prof. Paper, 440-kk, pp.1-12

Geophysical & Geochemical Prospecting Team of the Bureau of Geology & Mineral Resources of Guizhou Province (1988). A regional magnetic and gravity investigation in southwestern Guizhou Province: Scale 1:200000, Unpub. Internal Report.

Groves, D.I. (1993). The crustal continuum model for late-Archaean lodegold deposits of the Yilgarn Block, Western Australia. Mineralium Deposita, Vol. 28, No. 6, pp. 366-374, ISSN 0026-4598

Groves, D.I., Goldfarb, R.J., Gebre-Mariam, M., Hagemann, S.G. & Robert, F. (1998). Orogenic gold deposits: A proposed classification in the context of their crustal distribution and relationships to other gold deposit types. Ore Geology Reviews, Vol. 13, (April 1998), pp. 7-27, ISSN 0169-1368

Hall, D.L., Sterner, S.M. & Bodnar, R.J. (1988). Freezing point depression of NaCl-KCl-H2O solutions. Economic Geology, Vol. 83, (February 1988), pp. 197-202, ISSN 0361-0128

Heinrich, C.A. (2005). The physical and chemical evolution of low-salinity magmatic fluids at the porphyry to epithermal transition.A thermodynamic study. Mineralium Deposita, Vol. 39, No. 8, (February 2005), pp. 864-889, ISSN 0026-4598

Heinrich, C.A. & Eadington, P.J. (1986). Thermodynamic predictions of the hydrothermal chemistry of arsenic, cassiterite-arsenopyrite-base metal sulfide deposits. Economic Geology, Vol. 81, No. 3, (May 1986), pp. 511-529, ISSN 0361-0128

Herrmann, A.G. (1970). Yttrium and Lanthanides. In: Wedepohl, K.H. (Ed.), Handbook of Geochemistry, Vol. II/2. Springer-Verlag, Berlin, pp. 57-71. Section 39

Hofstra, A.H., Levethal, J.S., Northrop, H.R., Landis, G.P., Rye, R.O., Birak, D.J. & Dahl, A.R. (1991). Genesis of sediment-hosted disseminated-gold deposits by fluid mixing and sulfidization. Chemical-reaction-path modeling of ore-depositional processes documented in the Jerritt Canyon district, Nevada. Geology, Vol. 19, No. 1, (January 1991), pp. 36-40, ISSN 0091-7613

Hofstra, A.H., Zhang, X.C., Emsbo, P., Hu, R.Z., Su, W.C., Christiansen, W.D., Fu, S.W. & Theodorakos, P. (2005). Source of ore fluids in Carlintype gold deposits in the Dian-Qian-Gui area and West Qinling belt, P.R. China: Implications for genetic models, in Mao, J.W., and Bierlein, F.P., eds., Mineral deposits research: Meeting the global challenge: Heidelberg, Springer-Verlag, Vol. 1, pp. 533-536

Hofstra. H. & Cline J.S. (2000). Characteristics and models of Carlin-type gold deposits. Reviews in Economic Geology, Vol. 13, pp. 163-220, ISSN 07410123

Hou, Z.L. & Yang, Q.D. (1989). Discussion on metallogenic condition and model for micro-fine disseminated gold ore in the triangle area of Yunnan, Guizhou and Guangxi Province. Dizhi Zhaokuang Rencong, Vol. 4, No. 3, pp. 1-13 (in Chinese)

Huang, K.N. (1986). The petrological and geochemical characteristics and the tectonic setting of the Emeishan basalts in Kangdian craton and adjacent areas. unpub. PhD thesis (in Chinese)

Hu, R.Z., Su, W.C., Bi, X.W., Tu, G.Z. & Hofstra, A.H. (2002). Geology and geochemistry of Carlin-type gold deposits in China. Mineralium Deposita, Vol. 37, No. 3-4, (december 2001), pp. 378-392, ISSN 0026-4598

Ilchik, R.P. & Barton, M.D. (1997). An amagmatic origin of Carlin-type gold deposit. Economic Geology, Vol. 92, No. 3, (May 1997), pp. 269-288, ISSN 0361-0128

Kesler, S.E., Fortuna, J., Ye, Z.J., Alt, J.C., Zohar, D.P., Borhauer, J. & Chryssoulis, S.L. (2003). Evaluation of the role of sulfidation in deposition of gold, Screamer section of the Betze-Post Carlin-type deposit, Nevada. Economic Geology, Vol. 98, No. 6, (September 2003), pp. 1137-1157, ISSN 0361-0128

Li, W.K., Jiang, X.S., Ju, R.H., Meng, F.Y. & Zhang, S.X. (1989). The geological characteristics and metallogenesis of impregnated gold deposits in southwestern Guizhou, China, In: Collected Works of Regional Ore-forming Condition of Main Gold Deposit Styles in China, V.6 Southern Guizhou. Geological Publishing House Beijing, pp.1-86 (in Chinese)

Liu, J.Z. (2001). The geology of the Yanshang gold deposit, Zhenfeng county, Guizhou. Guizhou Geology, Vol. 18, pp. 174-178 , ISSN 1000-5943(in Chinese with English abstract)

Lu, Z.M. (1986). The activation of southwestern bordering of Yangtze paraplatform and the forming of Youjiang Geosyncline. Geology of Guizhou, Vol. 3, No. 1, pp. 9-27 , ISSN 1000-5943(in Chinese)

Mei, H.J. (1973). Petrochemical characteristics of two deep-derived trap in southwestern China and its relationship with iron and nickel mineralization. Geochemica, Vol. 1, No. 4, pp. 219-253(in Chinese)

Pettke, T., Diamond, L.W. & Kramers, J.D. (2000). Mesothermal gold lodes in the north-western Alps: A review of genetic constraints from radiogenic isotopes. European

Journal of Mineralogy, Vol. 12, No. 1, (January,February 2000), pp. 213–230, ISSN 0935-1221.

Pokrovski, G.S., Kara, S. & Roux, J. (2002). Stability and solubility of arsenopyrite, FeAsS, in crustal fluids. Geochimica et Cosmochimica Acta, Vol. 66, No. 13, (July 2002), pp. 2361-2378, ISSN 0016- 7037

Radtke, A.S., Rye, R.O. & Dickson, F.W. (1980). Geology and stable isotope studies of the Carlin gold deposit, Nevada. Economic Geology, Vol. 75, No. 5, (August 1980), pp. 641-672, ISSN 0361-0128.

Ressel, M.W., Noble, D.C., Henry, C.D. & Trundel, W.S. (2000). Dikehosted ores of the Beast deposit and importance of Eocene magmatism in gold mineralization of Carlin trend. Economic Geology, Vol. 95, No. 7, (November 2000), pp. 1417–1444, ISSN 0361-0128

Ridley, J.R. & Diamond, L.W. (2000). Fluid chemistry of orogenic lode gold deposits and implications for genetic models. Reviews in Economic Geology, Vol. 13, pp. 141–162, ISSN 0361-0128

Seward, T.M. (1973) Thio-complexes of gold in hydrothermal ore solutions. Geochimica et Cosmochimica Acta, Vol. 37, No. 3, (March 1973), pp. 379–399,ISSN 0016-7037

Sterner, S.M., Hall, D.L. & Bodnar, R.J. (1988). Synthetic fluid inclusions, V. Solubility relations in the system NaCl-KCl-H2O under vapor-saturated conditions. Geochimica et Cosmochimica Acta, Vol. 52, No. 5, (May 1988), pp. 989–1005, ISSN 0016-7037

Sun S.-S. & McDonough W.F. (1989). Chemical and isotopic systematics of oceanic basalts: Implication for the mantle composition and process. In Magmatism in the Ocean Basins (eds. Saunder A.D. and Norry M.J). Geological Society of London Special Publication, London, Vol. 42, pp. 313–345

Su, W.C., Hu, R.Z., Xia, B., Xia, Y. & Liu, Y.-P. (2009). Calcite Sm-Nd isochron age of the Shuiyindong Carlin-type gold deposit, Guizhou, China. Chemical Geology, Vol. 258, No. 3-4, (January 2009), pp. 269–274, ISSN 0009-2541

Su,W.C., Xia, B., Zhang, H.T., Zhang, X.C. & Hu, R.Z. (2008). Visible gold in arsenian pyrite at the Shuiyindong Carlin-type gold deposit. Guizhou, China: implications for the environment and processes of ore formation. Ore Geology Reviews , Vol. 33, No. 3-4, (June 2008), pp. 667–679, ISSN 0169-1368

Su,W.C., Heinrich, C.A., Pettke, T., Zhang, X.C., Hu, H.R., Xia, B., (2009). Sediment-hosted gold deposits in Guizhou, China: products of wallrock sulfidation by deep crustal fluids. Economic Geology, Vol. 104, pp. 73–93, ISSN 0361-0128

Su W.C, Zhang H.S, Xia B, Zhang X.C, Hu R.Z, Zhou G.F. & Xia Y. (2006). The first discovery of sub-micro and micro visible native gold grains in the Shuiyindong Carlin-type gold deposit in Guizhou. Acta Mineralogica Sinica, Vol. 26, No. 3, (September 2006), pp. 257–260, ISSN 1000- 4734(in Chinese with English abstract)

Tao, C.G., Liu, J.S. & Dan, G. (1987). On the gold ore deposit geological characteristics and genesis of Yata, Ceheng. Geology of Guizhou, Vol. 4, No. 2, pp. 135-150, ISSN 1000-5943(in Chinese)

Takenouchi, S. & Kennedy, A.C. (1964). The binary system H2O-CO2 at high temperatures and pressures. American Journal of Science, Vol. 262, (November 1964), pp. 1055–1074, ISSN 0002 -9599

Tödheide, K. & Franck, E.U. (1963). Das Zweiphasengebiet und die kritische Kurve im System Kohlendioxid-Wasser bis zu Drucken von 3500 bar.Zeitschrift für Physkalisoche Chemie Neue Folge, Vol. 37, pp. 387–401

Tretbar, D.R., Arehart, G.B., Christensen, J.N. (2000). Dating gold deposition in a Carlin-type gold deposit using Rb/Sr methods on the mineral galkhaite. Geology ,Vol. 28, No. 10, (October 2000), pp. 947–950, ISSN 0091-7613

Wang, Y.G., Suo, S.T. & Zhang, M.-F. (1994). Tectonics and Carlin-Type gold deposits in southwestern Guizhou. Geological Publishing House Beijing, pp. 115(in Chinese)

Wang, Y.G., Wang, L.T., Zhang, M.F. & Wang, L.L. (1995). Texture of the Upper crust and pattern of the disseminated gold deposits distributed in Nanpanjiang area. Guizhou Geology, Vol. 12, No. 2, pp. 91–183, ISSN 1000-5943(in Chinese with English abs.)

Xia Y. (2005). Study on the Metallogenic Characteristics and Gold Abnormal Enrichment Mechanism of the Shuiyindong Gold Deposit at Zhenfeng, Guizhou. Doctoral Dissertation of Post-graduate School of the Chinese Academy of Sciences

Yang, K.W. (1992). A preliminary discussion on the genesis of Getang gold deposit and its prospecting significance. Guizhou Geology, Vol. 9, No. 4, pp. 299-305 , ISSN 1000-5943 (in Chinese)

Yang, K.Y., Chen, F., Mei, H.J., Yang, K.W., Su, W.C., Zhang, X.C., Chen, S.M. & Feng, X.X. (1992). The investigation of ore-forming conditions and exploration for micro-grained disseminated gold deposits in southwestern Guizhou. Unpub, report of IGCAS Guiyang, pp. 96(in Chinese)

Ye, X.X., Wan, G.Q., Sun, Z.-Y., Liu, Y.-K., Zhou, L.-D., Liu, S.-R., Xue, D.-J., Rivers, L. & Jones, K.W. (1994). Microbeam analysis of gold in Carlintype gold deposits, southwestern Guizhou, China. Science in China (series B), Vol. 24, No. 8, pp. 883–889, ISSN 1674-7224(in Chinese)

Zhang, J., Lu, X.B., Yang, F.Q., Liao, Q.A., Wang, P., Wang, K.Y., Zhang, X.J., Wang, Q.W., Wang, H.M., Chen, K.L.. & Fu, S.H. (2002). Geology of Gold Deposits in Northwest China and Metallogenic Prognosis. Chinese University of Geology Press, Wuhan

Zhang, X.C., Spiro, B., Halls, C., Stanley, C. & Yang, K.Y. (2003). Sedimenthosted disseminated gold deposits in southwest Guizhou, PRC: Their geological setting and origin in relation to mineralogical, fluid inclusion, and stable-isotope characteristics. International Geology Review, Vol. 45, No. 5, pp. 407–470

Zang Yu, Xia Yong, Su Wenchao, Tao Yan, Zhang Xingchun, Liu Jianzhong & Deng Yiming. (2010). Metallogenic model and prognosis of the Shuiyindong super-large strata-bound Carlin-type gold deposit, southwestern Guizhou Province, China. Chinese Journal of Geochemistry, Vol. 29, (June 2010), pp.157–166, ISSN l000-9426.

Zhang Yu, Xia Yong, Wang Zepeng, Yan Baowen, Fu Zhikang & Chen Ming. REE and stable isotope geochemical characteristics of Bojitian gold deposit,Guizhou Province. Earth Science Frontiers, Vol. 17, No. 2, (Mach 2010), pp.385-395, ISSN 1005-2321. (in Chinese with English abstract)

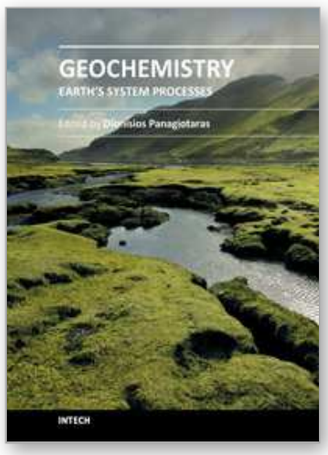

Geochemistry - Earth's System Processes

Edited by Dr. Dionisios Panagiotaras

ISBN 978-953-51-0586-2
Hard cover, 500 pages
Publisher InTech
Published online 02, May, 2012
Published in print edition May, 2012

This book brings together the knowledge from a variety of topics within the field of geochemistry. The audience for this book consists of a multitude of scientists such as physicists, geologists, technologists, petroleum engineers, volcanologists, geochemists and government agencies. The topics represented facilitate as establishing a starting point for new ideas and further contributions. An effective management of geological and environmental issues requires the understanding of recent research in minerals, soil, ores, rocks, water, sediments. The use of geostatistical and geochemical methods relies heavily on the extraction of this book. The research presented was carried out by experts and is therefore highly recommended to scientists, under- and post-graduate students who want to gain knowledge about the recent developments in geochemistry and benefit from an enhanced understanding of the dynamics of the earth's system processes.

How to reference

In order to correctly reference this scholarly work, feel free to copy and paste the following:

Yong Xia, Wenchao Su, Xingchun Zhang and Janzhong Liu (2012). Geochemistry and Metallogenic Model of Carlin-Type Gold Deposits in Southwest Guizhou Province, China, Geochemistry - Earth's System Processes, Dr. Dionisios Panagiotaras (Ed.), ISBN: 978-953-51-0586-2, InTech, Available from: http://www.intechopen.com/books/geochemistry-earth-s-system-processes/geochemistry-and-metallogenic-model-of-carlin-type-gold-deposits-in-southwest-guizhou-province-china

INTECH
open science | open minds

InTech Europe
University Campus STeP Ri
Slavka Krautzeka 83/A
51000 Rijeka, Croatia
Phone: +385 (51) 770 447
Fax: +385 (51) 686 166
www.intechopen.com

InTech China
Unit 405, Office Block, Hotel Equatorial Shanghai
No.65, Yan An Road (West), Shanghai, 200040, China
中国上海市延安西路65号上海国际贵都大饭店办公楼405单元
Phone: +86-21-62489820
Fax: +86-21-62489821

IntechOpen